TOPICAL REVIEW

Molecular beam epitaxy growth and scanning tunneling microscopy study of 2D layered materials on epitaxial graphene/silicon carbide

To cite this article: Hui Lu *et al* 2023 *Nanotechnology* **34** 132001

IOP Publishing Nanotechnology
Nanotechnology 34 (2023) 132001 (19pp) https://doi.org/10.1088/1361-6528/acae28

Topical Review

Molecular beam epitaxy growth and scanning tunneling microscopy study of 2D layered materials on epitaxial graphene/silicon carbide

Hui Lu[1,2], Wenji Liu[1], Haolin Wang[1], Xiao Liu[1,2], Yiqiang Zhang[3], Deren Yang[1,2] and Xiaodong Pi[1,2,*]

[1] State Key Laboratory of Silicon Materials & School of Materials Science and Engineering, Zhejiang University, Hangzhou, Zhejiang 310027, People's Republic of China
[2] Institute of Advanced Semiconductors & Zhejiang Provincial Key Laboratory of Power Semiconductor Materials and Devices, ZJU-Hangzhou Global Scientific and Technological Innovation Center, Hangzhou, Zhejiang 311200, People's Republic of China
[3] School of Materials Science and Engineering & College of Chemistry, Zhengzhou University, Zhengzhou, Henan 450001, People's Republic of China

E-mail: xdpi@zju.edu.cn

Received 29 August 2022, revised 10 November 2022
Accepted for publication 23 December 2022
Published 17 January 2023

Abstract

Since the advent of atomically flat graphene, two-dimensional (2D) layered materials have gained extensive interest due to their unique properties. The 2D layered materials prepared on epitaxial graphene/silicon carbide (EG/SiC) surface by molecular beam epitaxy (MBE) have high quality, which can be directly applied without further transfer to other substrates. Scanning tunneling microscopy and spectroscopy (STM/STS) with high spatial resolution and high-energy resolution are often used to study the morphologies and electronic structures of 2D layered materials. In this review, recent progress in the preparation of various 2D layered materials that are either monoelemental or transition metal dichalcogenides on EG/SiC surface by MBE and their STM/STS investigations are introduced.

Keywords: molecular beam epitaxy, epitaxial graphene/silicon carbide, scanning tunneling microscopy/spectroscopy, two-dimensional layered materials

(Some figures may appear in colour only in the online journal)

1. Introduction

Recently, with the development of study on graphene, a number of new graphene-like single layered (SL) two-dimensional (2D) materials have been successfully fabricated such as silicene, germanene, black phosphorus, stanene, transition metal dichalcogenides (TMDs) [1, 2]. These 2D materials have exotic physical properties such as thermoelectric effect, superconductivity, and quantum spin Hall (QSH) effect. And they possess huge potential in field-effect transistors, optoelectronic devices, energy storage and other fields [3–5]. Furthermore, 2D materials also can be used as templates to prepare various heterostructures with excellent properties [6].

There are various modern techniques to fabricate SL 2D layered materials such as exfoliation methods, chemical vapor deposition (CVD) and molecular beam epitaxy (MBE) Up to now, with the development of exfoliation methods a variety of 2D layered materials such as WSe_2, MoS_2 and graphene were

* Author to whom any correspondence should be addressed.

acquired [7–9]. However, the surface quality of 2D materials may be damaged during the process and some residual contamination may also remain on the surface, which will affect their electrical properties [10]. The disadvantage of CVD is the requirement of very high growth temperature, which will result in many vacancies in 2D materials. Compared with the above two methods, the advantage of MBE is that high quality monolayer (ML) 2D layered materials with a clean surface can be obtained by layer-by-layer growth mode under low growth temperature and ultra-high vacuum (UHV) [11]. Moreover, MBE is a dynamic process instead of thermodynamic equilibrium condition, it can fabricate some important naturally non-existent or unstable 2D materials including silicene [12], bismuthene [13], blue phosphorus [14], and so on. Substantially, most 2D materials are synthesized by epitaxial growth on metal substrates [15–17]. Unfortunately, due to the strong interaction between 2D materials and metal substrates, the intrinsic physical properties of free ML 2D materials are destroyed, resulting in the limited application of the 2D materials. For example, it is found that the Dirac cone disappears at Fermi level because of the strong hybridization between graphene, silicene and germanene and the metal substrates [18–20]. Moreover, 2D layered materials may be unstable when growing on the metal substrates [21]. Therefore, there is an urgent need to find a substrate that can preserve the intrinsic properties of 2D materials. As the first 2D layered materials, graphene has attracted significant interests due to its exotic physical properties. Graphene-based materials have been considered as star materials for a lot of applications, ranging from transistors, capacitors to batteries [22–24]. Actually, graphene is also considered as an excellent candidate substrate for epitaxial growth of 2D materials for following reasons [25]. (i) Graphene can be fabricated on SiC by flash annealing under UHV, and graphene sticks to the SiC surface like a carpet. The work function may vary due to the presence of different layers of graphene on SiC surface [26]. Compared with HOPG, inhomogeneities of the EG/SiC substrate may provide more nucleation sites for the synthesis of uniform ML 2D material layers. (ii) Graphene can be used as an excellent substrate for epitaxial growth of layered 2D materials due to its chemically inertness [27]. The weak interaction between graphene and epitaxial materials [28] can reduce the strain effect and help to preserve the intrinsic characteristics of 2D materials. (iii) Epitaxial materials can be easily removed from the graphene surface and transferred to any desired substrates surface [29]. Besides, 2D materials on EG/SiC can be directly applied without further transfer to other substrates [30, 31]. Therefore, EG/SiC is regarded as a promising substrate for the epitaxial growth of 2D layered materials. In addition, because of its high spatial resolution and high energy resolution, STM has given a vast and valuable contribution to obtain the morphologies and electronic structures of 2D materials. This technique has been employed to obtain various features of 2D materials. For instance, identifying different phases [32–34], studying charge density waves [35–37], mapping low density of states (DOS) [38, 39], observing quasiparticle interference [40–42] and edge states [43]. Thus, STM is considered as a promising tool to measure the 2D materials.

In this review, we summarize the research progress of MBE-grown 2D layered materials on EG/SiC surface, which are either monoelemental (e.g. silicene, bismuthene, tellurene) or TMDs. The morphologies and the electronic properties of these 2D layered materials have been measured with STM/STS. We hope this review can help the readers to understand the 2D layered materials and gain experience from previous researches.

2. Monoelemental 2D layered materials

2.1. Silicene

Silicon and carbon both belong to group-IV on the periodic table and play significant roles in materials science. However, the crystal structures of carbon and silicon are different. Carbon atoms are hybridized with sp^2 to form layered graphite, and silicon atoms are hybridized with sp^3 to form a face-centered cubic diamond structure. With the realization of graphene with atomic layer thickness, the 2D structure of silicon with monoatomic layer thickness receives more and more attention from researchers [44, 45]. Wang *et al* defined the 2D honeycomb silicon monoatomic layer formed by sp^2 hybridization as silicone [44]. Figure 1(a) is a 2D representation of the lattice.

Silicene is the silicic version of graphene [45], which has a similar energy band structure with graphene. It has a Dirac electronic structure analogous to graphene, and its Brillouin zone also has 6 linear dispersion Dirac cones [46]. Silicene has many quantum effects similar to the graphene system, while the sp^2 and sp^3 hybridization between silicon atoms give silicene a unique warped structure. Besides, silicene also possesses a spin–orbit coupling energy gap of 1.5 meV, which can realize the QSH effect [47].

The novel physical properties of silicene have attracted more and more researchers to use various experimental techniques to prepare it. Several groups have achieved the 2D growth of silicene via MBE [11, 48]. Usually, silicene is prepared on the metal substrates. However, density functional theory calculation and STM study demonstrate that a strong Si-Metal interaction must be considered [49]. Whether pure 2D silicene is actually obtained remains controversial. Therefore, it is worth a shot to grow silicene on a relatively inert substrate like EG/SiC.

Sone *et al* studied the growth of Si on EG/6H-SiC(0001) [50]. Unfortunately, 2D silicene has not been observed on graphene surface. At 290–420 K, distinctive flower-like islands are formed, as shown in figure 1(b). They found that the growth was mainly controlled by diffusion-limited aggregation, and monatomic silicene wasn't obtain on surface. They attributed this result to the weak interaction between the graphene substrate and Si adatoms. Therefore, they considered silicene cannot grow on EG/SiC.

However, Berbezier *et al* have successfully grown large nanostructures of silicene on graphene covered 6H-SiC (0001) which turn out to be a good template [51]. The results are not consistent with previous report. Silicene (as shown in

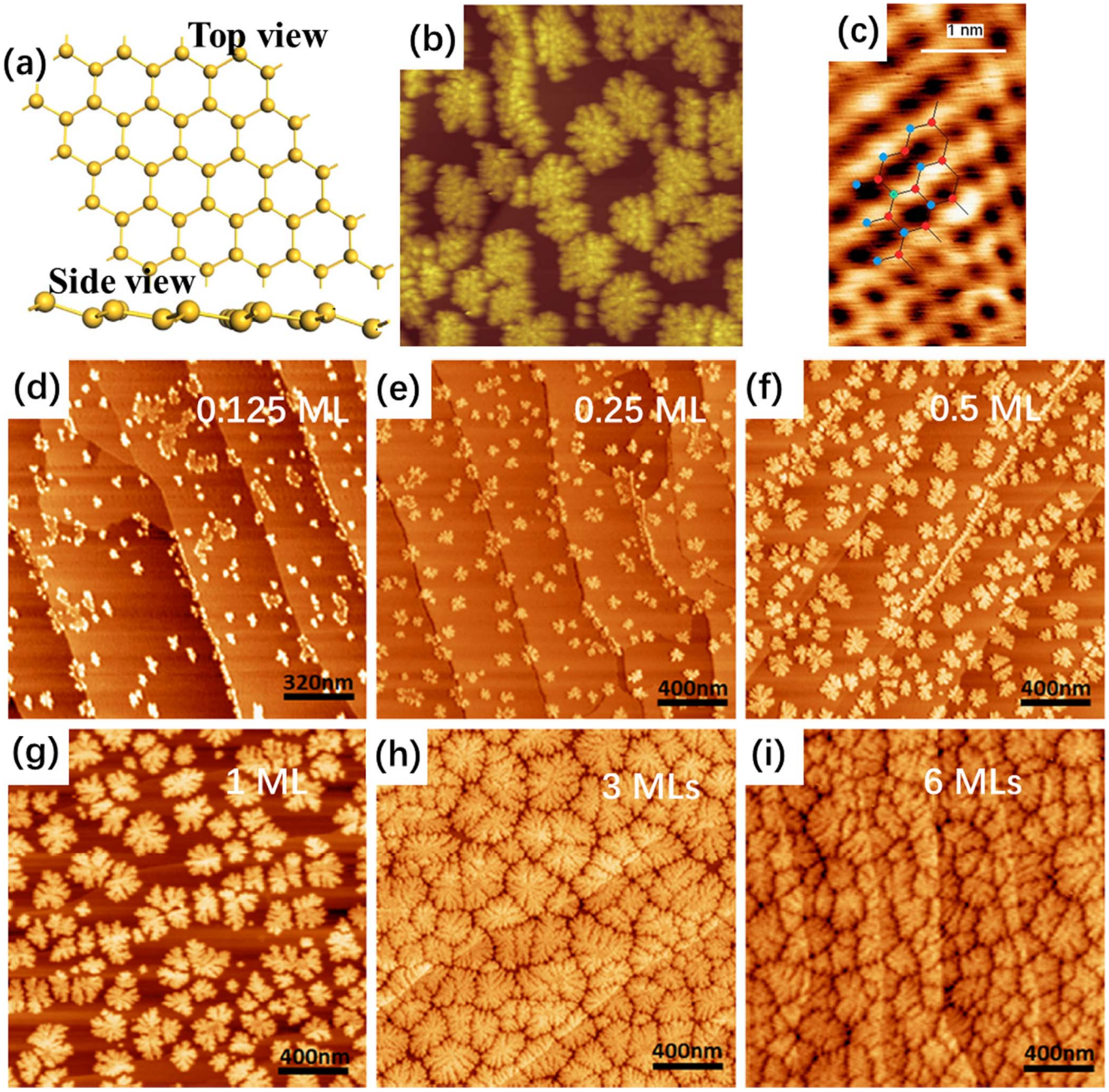

Figure 1. (a) The lattice structure of silicene from top and side view. Reprinted from [44], Copyright (2015), with permission from Elsevier. (b) Morphology of flower-like islands on EG/6H-SiC surface (240 × 240 nm^2). Reproduced from [50]. © IOP Publishing Ltd. All rights reserved. (c) STM image of silicene on EG/SiC and a stick-and- model ball is superimposed. Red, blue and green atoms represent Si atoms. Reproduced from [51]. Used with permission of World Scientific Publishing Co., Inc., from Silicene Nanostructures Grown on Graphene Covered SiC (0001) Substrate Int. J. Nanosci. 18 1940039, permission conveyed through Copyright Clearance Center, Inc. AFM images of the surface after Si deposition at RT on EG/6H-SiC (0001) of different thickness (d) 0.125 ML; (e) 0.25 ML; (f) 0.5 ML; (g) 1 ML; (h) 3 ML; (i) 6 ML. Reprinted with permission from [52]. Copyright (2022) American Chemical Society.

figure 1(c)) shows an almost complete sp^2 configuration with a very small buckling according to the STM image. And the STS results further confirm the silicene is metallic. Recently, Berbezier *et al* reported that large-scale quasi-free-standing silicene can be fabricated on CVD EG/6H-SiC at small deposited thicknesses of silicon layers (<1 ML) [52]. They considered that two conditions were essential for epitaxial growth large-scale silicene sheets on EG/6H-SiC: defect-free 1 ML graphene and the UHV environment. At low coverages (<1 ML), 2D silicene sheets were observed on surface by atomic force microscope (AFM) and the 2D silicene sheets were surrounded by 3D ridges forming dendritic islands (figures 1(d)–(f)). After 1 ML deposition, the 2D silicene sheets totally disappeared and large-scale 3D dendritic island appeared (figure 1(g)). At high coverages (from 3 to 6 ML), the surfaces were fully covered by dendrites (figures 1(h)–(i)). They considered that the Si atoms on the first layer were only weakly bonded to the graphene and the diffusion barrier was

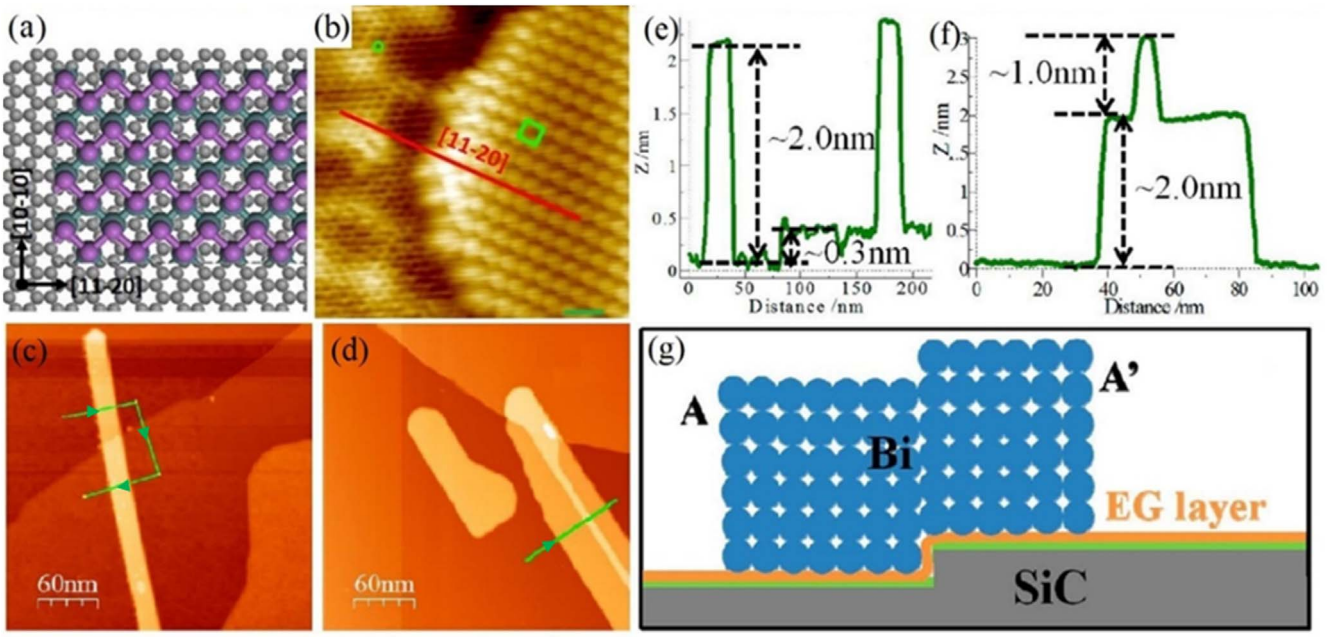

Figure 2. (a) Possible arrangement of Bi thin films on ML EG. The purple and black balls represent Bi atoms, gray balls represent C atoms. (b) The atomic scale of Bi films on ML EG. Reprinted with permission from [64]. Copyright (2014) American Chemical Society. (c) and (d) Morphologies of Bi nanoribbons grown across EG steps. (e) and (f) Height profiles along the green arrows in figures (c) and (d). (g) Proposed mode of one Bi nanoribbon grown across EG steps. Orange and green lines represent EG layer and buffer layer, respectively. Reprinted with permission from [65]. Copyright (2018) American Chemical Society.

low. However, Si atoms diffusing on top of the deposited Si layers the energy barrier became greater due to strong Si–Si interactions.

2.2. Bismuthene

Bismuth (Bi) is a semimetal and possesses exotic electron distribution, which endows Bi with various interesting physical properties [53–56]. In contrast to the bulk Bi, Bi nanostructures have many unique properties, such as surface superconductivity [57], and transformation from semimetal to semiconductor [58]. In addition, splitting of surface-state bands can be observed on Bi surface, which show potential application in spintronics [59]. Bismuthene on a SiC has been considered as a promising 2D materials for the high temperature QSH structure [12]. Bi films and nanostructures have been fabricated on various substrates, such as HOPG [60], Si(111) [61], Bi_2Te_3/Si [62] and metal substrates [63]. However, there are few studies on the epitaxial growth of the Bi films and nanostructures on EG/SiC.

Fabrication of metal nanostructures on EG is essential for its practical applications. The growth of Bi nanostructures on the EG/SiC surface has been initially investigated by Huang *et al* [64]. The results depict the physically-adsorbed nature of Bi nanostructures on EG/SiC. The proposed model is shown in figure 2(a) and the atomic scale of Bi nanostructures on ML EG is displayed in figure 2(b). As Bi coverage area increased, graphene-related peaks are almost unvaried according to photoemission spectroscopy results. They demonstrated that Bi nanostructures on EG surface was an islanding growth pattern because of weak interface interaction. In addition, due to quantum and size effects, the Bi nanostructures exhibit semiconducting properties.

Besides, Ma *et al* reveled that Bi nanoribbons and nanorods are prone to grow at different places of EG/SiC surface [65]. Nanorods tend to grow on SiC buffer layer and the diffusion barrier is very high. However, Bi nanoribbons prefer to grow on ordered EG. They obtained a Bi nanoribbon, which grew across EG steps in figures 2(c) and (d). The heights of the EG step and the Bi nanoribbon is shown in figures 2(e) and (f). Moreover, they displayed proposed growth mode of the Bi nanoribbon across EG steps in figure 2(g). Since growth of the Bi nanoribbon can extend across EG steps, a continuous 2D growth mode is proved.

Hu *et al* found that Bi atoms could tune the defects of EG on SiC surface [66]. Bi atoms were firstly deposited on SiC surface before the fabrication of EG to facilitate single defects and defect clusters, then Bi atoms were thoroughly cleaned away at higher temperature by post-annealing. Ultimately, defects could be fabricated on graphene. The results reveal the potential of Bi atoms on defect engineering as well as on applications in electronics of Bi atoms.

2.3. Tellurene

Layered tellurium (Te) is a semiconductor with various exotic physical properties, such as tunable bandgap [67], superconductivity [68], high hole mobility [69], excellent optical response [70], and so on, motivating researchers to study on ML Te films. Although many kinds of Te nanostructures have been synthesized in previous reports [71–73], the epitaxial growth of Te films on EG/SiC is still rarely reported.

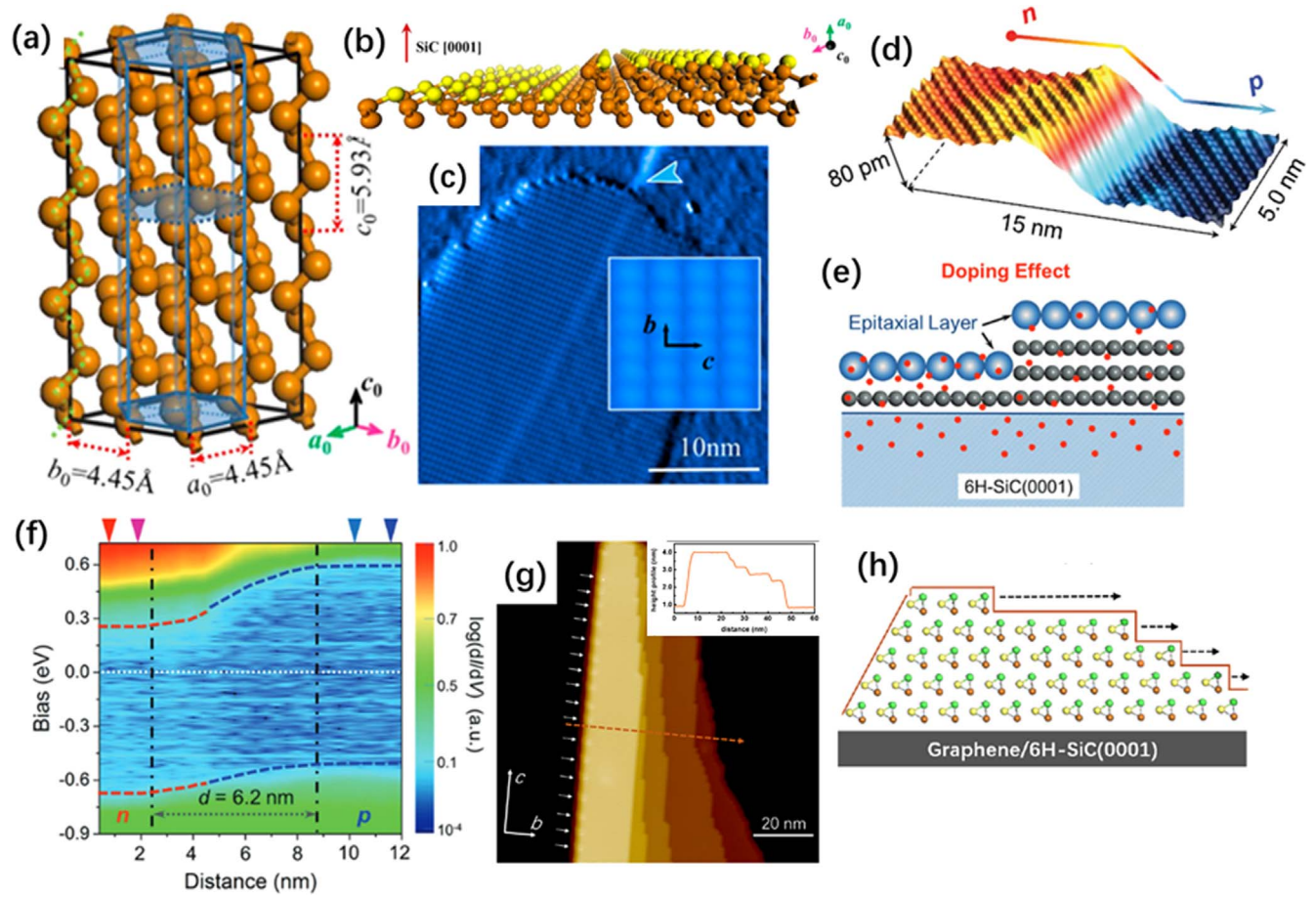

Figure 3. (a) and (b) Schematic diagram of Te crystal structure and BL Te films, respectively. Orange and yellow balls represent Te atoms, respectively. (c) STM image of SL Te film. Reprinted with permission from [74]. Copyright (2017) American Chemical Society. (d) The *p*–*n* junction of ML Te across the graphene steps. (e) Schematic diagram of electron doping effect. (f) The dI/dV mapping of the step edge. [76] John Wiley & Sons.© 2018 WILEY-VCH Verlag GmbH & Co. KGaA, Weinheim. (g) STM image of Te nanoribbon on EG/SiC. Inset: height profile along the dashed orange arrow. (h) The film-growth mode of Te layers in the nanoribbon on EG/SiC substrate. Reprinted figure with permission from [75], Copyright (2021) by the American Physical Society.

In 2017, Huang *et al* firstly fabricated ML and few-layer Te films on EG/6H-SiC surface via MBE [74]. Figures 3(a) and (b) are schematic diagrams of 3D configuration of the Te crystal and the bilayer (BL) Te on EG/6H-SiC surface, respectively. They obtained the atomic structure of the SL Te films in figure 3(c) and also revealed that the Te films were composed of many parallel chiral Te chains [75]. Moreover, the bandgap of Te was negatively correlated with thickness. When thickness decreases, the bandgap increases monotonically up to 0.92 eV for the ML Te. Therefore, with controllable thickness in ML, Te films will display great potential in optoelectronic application.

Besides, the band structure of Te films was also investigated. Huang *et al* found that at the edge of ML Te films and EG the bending was upward band in the dI/dV mapping (figure 3(f)) [76]. This result also indicated that the electronic and optoelectronic properties of Te films could be tuned. Then, they successfully fabricated the in-plane *p*–*n* junctions across the graphene steps, as shown in figure 3(d). They found that the doping effect of SiC substrate depended on the thickness of overlaid graphene. STS measurements revealed that Te film showed a *p*-type behavior on trilayer graphene, but it showed a *n*-type behavior on single layer graphene (SLG), and the corresponding schematic diagram was shown in figure 3(e).

Defects with a small scale periodic at edges of Te nanoribbons were synthesized later [75]. Guo *et al* found that Te nanoribbons were chiral and quasiperiodic defects induced modulation of electronic states was quasiperiodic. The energy gap was enhanced at the site of defects and recovered away from the defects. An STM image of Te nanoribbon on EG/SiC is shown in figure 3(g), in which both edges along the chain direction can be revealed. The Te films composing the Te nanoribbon are aligned together at one edge along one direction, while they are misaligned at the opposite edge. Based on the topographic characteristics and theoretical calculations, they considered that the Te films in the nanoribbon had a preferred growth mode from the aligned edge, as shown in figure 3(h).

3. Transition metal dichalcogenides

3.1. $MoSe_2$

MoS_2 is one of the best known 2D-TMDs materials due to its application potential in optoelectronic synapses and

transistors [77, 78]. The main reason is that the bandgap of MoS_2 depends on the thickness and MoS_2 can transform from indirect to direct band gap semiconductor [79–81]. The underlying substrate also has important influence on the electrical properties of MoS_2/graphene heterostructures. At present, CVD and mechanical exfoliation methods are mostly used for MoS_2 epitaxy on EG/SiC, but MBE method is rarely used. Therefore, in this review we do not give a detailed description of epitaxial growth of MoS_2 by MBE In addition to MoS_2, another layered 2D materials, $MoSe_2$ is also studied extensively. For example, SL $MoSe_2$ has great application potential in optoelectronics devices and electronic devices [82–84]. Compared with MoS_2, SL-$MoSe_2$ has many unique properties. SL-$MoSe_2$ has a narrower direct band gap, so it can be used in photoelectrochemical cells and single junction solar cells [85–87]. Schematic of layered $MoSe_2$ on EG/SiC surface is shown in figure 4(a). Each SL-$MoSe_2$ contains two Se atomic layers and one Mo atomic layer is inserted in the middle [86]. SL $MoSe_2$ synthesized by MBE has been reported to grow on different substrates including Au(111) [88] and EG/SiC [89]. It is found that $MoSe_2$ can transform from indirect in bulk to direct band gap semiconductor in ML. Crommie *et al* also used STM/STS to measure the morphology and electronic properties of ∼0.8 ML $MoSe_2$ films grown on EG/SiC by MBE [86]. Due to only submonolayer $MoSe_2$ on surface, the $MoSe_2$ films and the underlying BLG can be characterized simultaneously using STM (figures 4(b) and (c)). They found that $MoSe_2$ on BLG surface had a honeycomb lattice structure and a Moiré pattern, and renormalized bandgap and excitonic effects can be observed in ML $MoSe_2$. The Moiré pattern arises from lattice mismatch the distinct lattice parameters of $MoSe_2$ and graphene, as well as their relative stacking orientation.

Crommie *et al* revealed that the electronic properties of $MoSe_2$ film were thickness dependent through STS measurements [90]. They fabricated a sample with the layer number of ML, BL and TL shown in figure 4(d). A series of the STS spectra for $MoSe_2$ with different thickness are shown in figures 4(e)–(g) and the distinct features appear in both the valence band (VB) and conduction band (CB). A wide bandgap is surrounded by the band edges (V1, C1) and the CB (C1, C2), are indicated in the figures 4(e)–(g), respectively. The corresponding bandgap values are marked on a logarithmic scale (figures 4(h)–(j)). These results clarified the influence of thickness on the electronic properties of $MoSe_2$. Wu *et al* demonstrated that SL-$MoSe_2$ was a direct bandgap semiconductor with 1.55 eV and had good thermal stability [91]. The photoluminescence (PL) peak height decreased rapidly from SL to bulk, demonstrating the transition from direct band in the SL to the indirect bandgap in the bulk (figure 4(k)), which was similar to MoS_2 [92]. Moreover, the electrical energy (1.86 eV) of SL-$MoSe_2$ is in the wavelength range of visible light, which endows SL-$MoSe_2$ with an important application value in photocatalysis and solar cells. Jamet *et al* found that the interaction between the $MoSe_2$ and few-layer graphene could help the graphene to open a band gap. The band gap is about 250 meV, and they believed that it was due to an interface charge transfer that leads to an electronic depletion in the few-layer graphene [93]. Besides, Barja *et al* found isolated 1D charge density wave (CDW) at mirror twin boundaries of SL-$MoSe_2$ films [89].

The crystalline structures and the device performance of the 2D-TMD semiconductors can be affected by various defects such as vacancies, adatoms and grain boundaries [94, 95]. The chalcogen atom substitution is also considered as a typical defect in 2D-TMD semiconductors, such as oxygen-substituted MoS_2 and oxygen-substituted $MoSe_2$ [96, 97]. In 2019, Barja *et al* observed the morphology and electronic structure of the point defects in ML $MoSe_2$ on EG/SiC grown by MBE through AFM and STM/STS measurements [97]. After gentle annealing, they found chalcogen defects appeared as the vacancies in AFM image (figure 4(l)), but the theoretical calculations predicted that theses defects as substitutional oxygen chalcogen sites did not appear deep in-gap states in the bandstructure, these results were consistent with the STS data (figure 4(m)). This work revealed that substitutional oxygen as point defects in 2D-TMDs, not just chalcogen vacancies.

3.2. WSe_2

WSe_2 possesses large spin-splitting in the VB among the TMDs semiconductors [98], which makes WSe_2 has great application potential in spintronic devices [99, 100]. Similar to other layered TMDs, the ML WSe_2 is also a sandwich structure and the atomic structure is shown in figure 5(a) [101]. It is found that ML WSe_2 is the first TMDs material that can possess both *p*-type and *n*-type conductive properties [102].

Initially, researchers utilized mechanical exfoliation and CVD methods to fabricate atomically thick WSe_2 nanosheets. However, the quality of WSe_2 is poor. Until 2013, Xie *et al* utilized MBE-grown atomically flat ML and BL WSe_2 films, and the films had no domain boundary (figure 5(b)) [103]. They also acquired the STS spectra of ML and BL WSe_2 domains. They found that the bandgap increased from BL to ML and a band-bending effect appeared in the boundary. In one report, Mo *et al* have reported the grown of WSe_2 films on EG via MBE and have analyzed the electronic structure. Angle-resolved photoemission spectroscopy (ARPES) and STS measurements reveal that electronic properties of WSe_2 are thickness dependent and WSe_2 films are *n*-type doping on EG/SiC [104]. In another report, Zhen *et al* acquired the PL spectra of ML WSe_2 and the WSe_2/graphene heterostructure in figure 5(c) [105]. The PL intensity of pristine ML WSe_2 is more than 15 times stronger than that of WSe_2/graphene heterostructure, indicating that interlayer relaxation of WSe_2/graphene heterostructure is more than 15 times fasters than that of intralayer recombination in ML WSe_2.

Besides, Chiang *et al* successfully fabricated a quasi-freestanding 1T′-WSe_2 films on BLG that did not appear in the bulk [106]. Using ARPES and STM/STS, they found a gap of 129 meV in this 1T′-WSe_2 films (figure 5(d)) and it was suitable for QSH electronics at RT. Moreover, Qian *et al* also demonstrated that the 1T′-WSe_2 films prepared on EG/SiC was more suitable for fabrication of topological field effect transistors [107]. In 2020, Li *at al* successfully

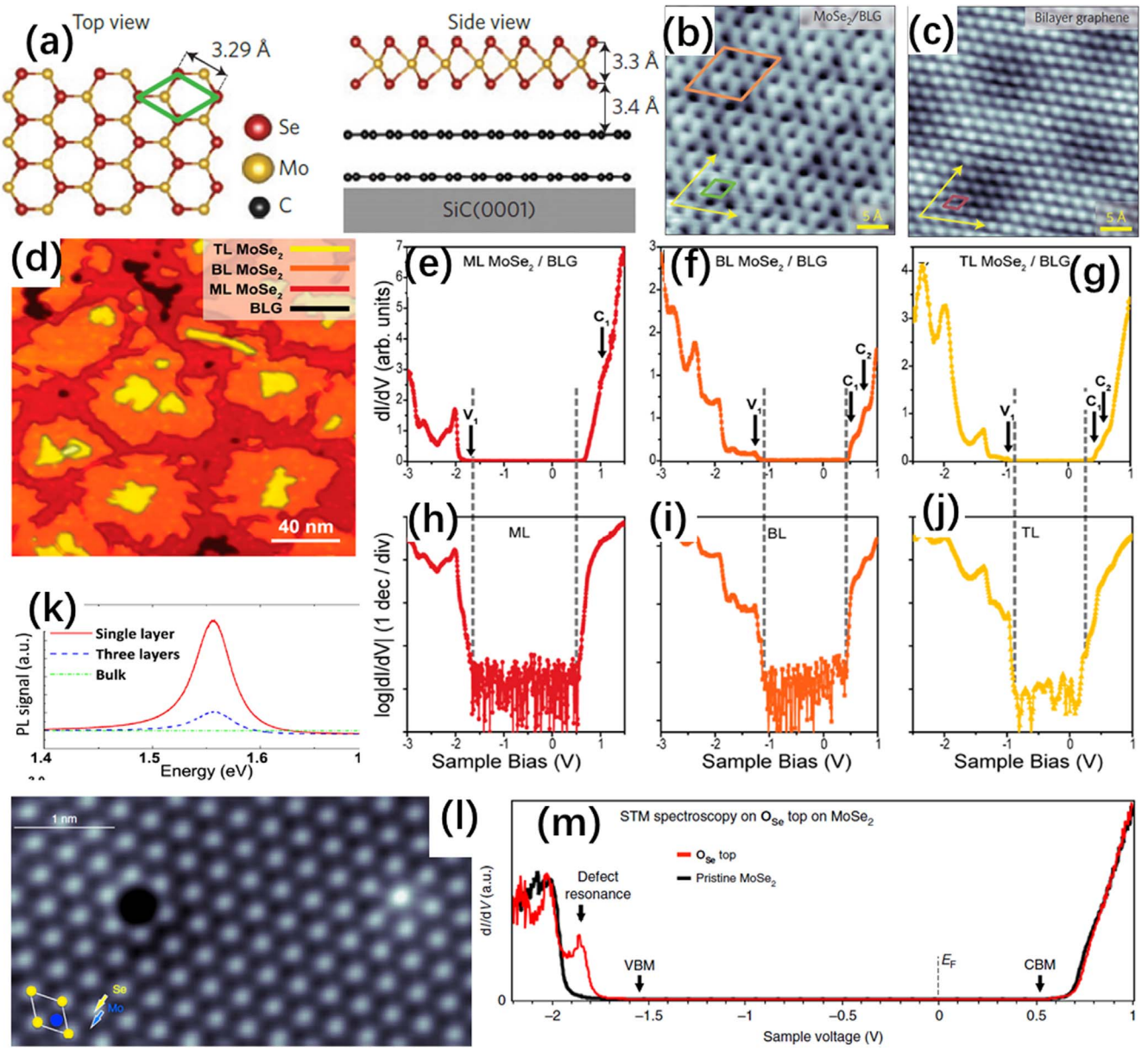

Figure 4. (a) Structure of $MoSe_2$ on BLG/SiC surface. (b), (c) STM images of ML $MoSe_2$ and BLG, respectively. Yellow arrows represent the orientation of the graphene lattice. The unit cells are indicated in green, dark red and orange for $MoSe_2$, BLG and a Moiré pattern. Reproduced from [86], with permission from Springer Nature. (d) A sample with different layers of $MoSe_2$. (e)–(g) STS spectra obtained for $MoSe_2$ with different thickness. (h)–(j) are the logarithmic scale of (e)–(g). Reproduced from [90]. CC BY 4.0. (k) PL spectra of the SL, TL and bulk $MoSe_2$. Reprinted with permission from [91]. Copyright (2012) American Chemical Society. (l) AFM image of Q_{se} (substitutional oxygen at a Se site) in 2D-$MoSe_2$; (m) STS spectra of the left defect in figure 4(l) Q_{se} and pristine $MoSe_2$. Reproduced from [97]. CC BY 4.0.

fabricated 1T′-1H WSe_2 lateral heterojunctions on EG/SiC and found edge state at the heterojunctions, which will be advantageous to prepare nano quantum devices [108]. Ugeda *et al* observed the topologically protected states at boundaries in SL 1T′-1H WSe_2 [109]. They displayed the STS spectra acquired at the bulk of 1T′ phase and at the edge of 1T′-1H interface in figure 5(e) and found 1T′ bulkgap disappeared at distances greater than 2 nm from the 1T′-1H interface. The appearance of the peak in the edge indicated that the existence of a topologically protected state. They also mapped the dI/dV near 1T′-1H interface in figure 5(f) and revealed that the interface state could penetrate into the 1T′-WSe_2 bulk. Quang *et al* demonstrated that charged defects and edges in $MoSe_2$ and WSe_2 deposited on EG/SiC could lead to band bending [110]. In addition, Liu *et al* revealed that the edge states at W edges were depended on the number of additional Se atoms, while the edge states at Se edge were always been observed [111]. These results demonstrate the influence of edge terminations on the edge states in WSe_2, significant for tailoring the electronic properties of TMD-material-based electronic devices in future.

3.3. $PtSe_2$

Platinum disselenide ($PtSe_2$) also has high charge-carrier mobility and wide bandgap and it is a new type of TMDs

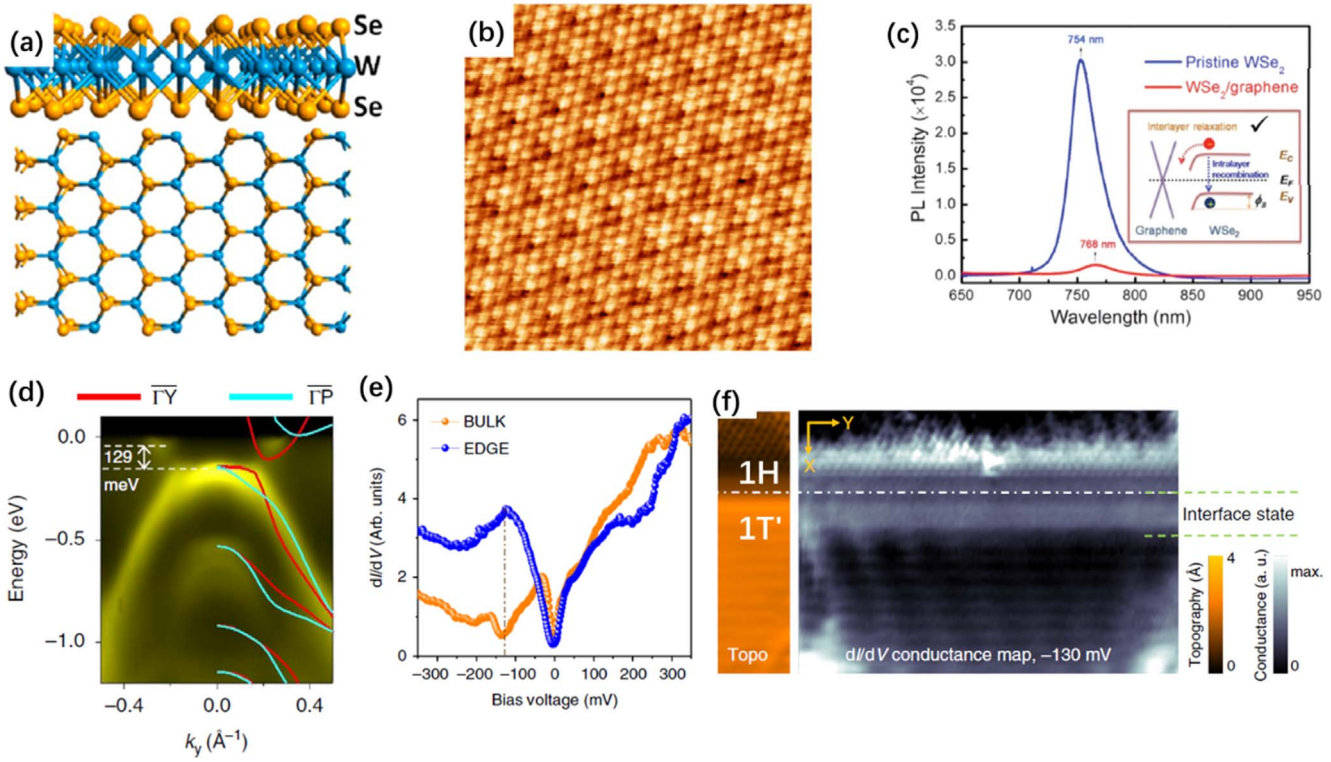

Figure 5. (a) The structures of the ML-WSe_2. Reprinted with permission from [101]. Copyright (2013) American Chemical Society. (b) Surface morphology of the ML-WSe_2 on graphene. Reproduced from [103]. © IOP Publishing Ltd. All rights reserved. (c) PL spectra of ML WSe_2 and ML WSe_2/graphene heterostructure. The inset indicates the interlayer relaxation at the heterointerface and the intralayer recombination in ML WSe_2. Reproduced from [105], with permission from Springer Nature. (d) ARPES data of 1T′-WSe_2. The red and blue lines computed bands for the mixed-domain configurations. Reproduced from [106], with permission from Springer Nature. (e) STS spectra obtained at the bulk of 1T′ phase and at the edge of 1T′-1H interface. (f) STM image and corresponding dI/dV map of the 1T′-1H interface. Reproduced from [109], with permission from Springer Nature.

[112]. Although the atomic structure of $PtSe_2$ is also typical sandwich structure, its stable phase is 1T, which is different from other layered TMDs. The building block of $PtSe_2$ is shown in figure 6(a) [113]. Bulk $PtSe_2$ is a semimetal, but ML $PtSe_2$ is a semiconductor and the bandgap is about 1.20–2.10 eV [114, 115]. Thus, the electronic properties of $PtSe_2$ also can be controlled by changing the number of $PtSe_2$ layers. Besides, compared with traditional $PtSe_2$ nanocrystals, ML $PtSe_2$ has an excellent photocatalysis property.

Initially, $PtSe_2$ films were prepared using MBE by direct selenization of Pt(111) substrate and this method can yield millimeter size $PtSe_2$ films(figure 6(b)) [115].

However, the electronic properties of $PtSe_2$ films are affected by the metallic Pt substrates, which impedes its application in electronic devices. In addition, this method can only produce ML $PtSe_2$ films, but it is difficult to acquire thicker $PtSe_2$ films. Subsequently, Zhou *et al* reported that they obtained $PtSe_2$ films from 0.8 to 22 ML on BLG/SiC substrate by MBE [113]. The topographic characteristic of the 0.8 ML $PtSe_2$ is shown in figure 6(c). In order to investigate the relationship between the electronic structure and the film thickness, they also obtained low-energy electrondiffraction (LEED) and ARPES results taken from 1 to 22 ML $PtSe_2$ in figures 6(d)–(m). In figure 6(d), both the 1 ML $PtSe_2$ film and the graphene substrate can be observed. As the thickness of $PtSe_2$ increase, the substrate surface is completely covered by $PtSe_2$ and the signal of graphene substrate disappears in the LEED pattern. According to the ARPES result of 1 ML $PtSe_2$ film (figure 6(i)), it can be seen that 1 ML $PtSe_2$ is a semiconductor and the bandgap is 1.2 eV. As predicted, when the thickness of $PtSe_2$ is thicker than 1 ML, ARPES results show that the bandgap of $PtSe_2$ film is decreasing [116]. However, when the $PtSe_2$ film thickness increases to 22 ML, the ARPES result is as same as the bulk $PtSe_2$. All the ARPES results indicate that the bandgap of the $PtSe_2$ films can be tuned by film thickness.

The $PtSe_2$ thin films can also be epitaxially grown on the insulating substrates surface. Moreover, due to its air stability and excellent electrical properties, $PtSe_2$ film will be considered as a promising candidate material in electronic devices in the future.

3.4. VSe_2

Vanadium diselenide (VSe_2), a typical layered TMDs, the crystal structure is shown in figure 7(a) [117]. Vidya *et al* reported that when VSe_2 films were grown on BLG/SiC surface, different growth temperatures would result in different polymorphs [118]. At growth temperature of 200 °C, the ML VSe_2 film displays a 2D incommensurate CDW patterns (figure 7(b)). Then, it can evolve into a commensurate $4a \times 4a$ CDW in the BL VSe_2 (figure 7(c)). However, at

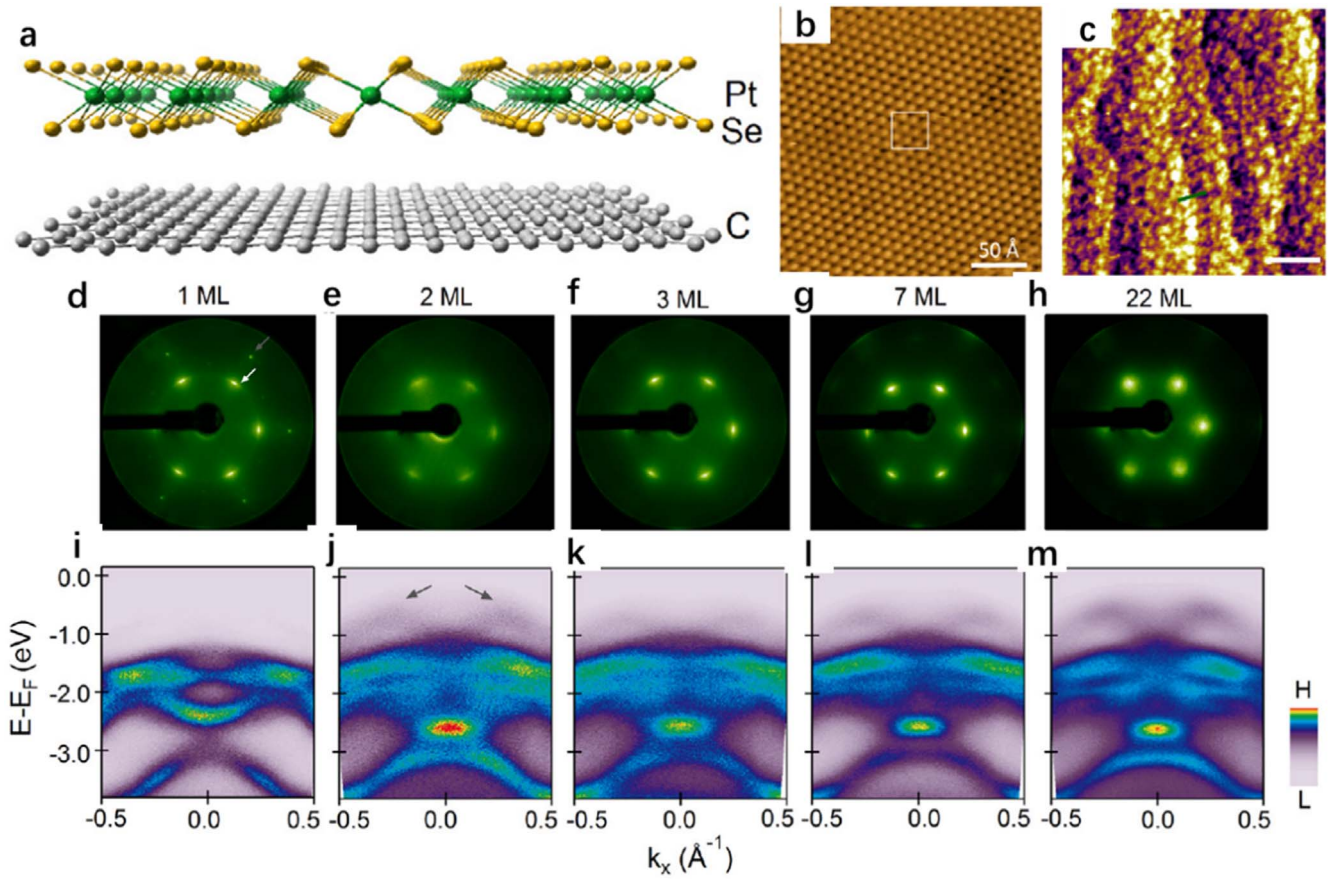

Figure 6. (a) Structure of $PtSe_2$ on EG surface. Reproduced from [113]. © IOP Publishing Ltd. All rights reserved. (b) STM image of $PtSe_2$ on Pt(111). Reprinted with permission from [115]. Copyright (2015) American Chemical Society. (c) Surface structure of 0.8 ML $PtSe_2$ on EG/SiC surface. LEED data of $PtSe_2$ films from 1 to 22 ML(d)–(h) and corresponding ARPES data acquired along the Γ–*K* direction taken at 21.2 eV (i)–(m). Reproduced from [113]. © IOP Publishing Ltd. All rights reserved.

growth temperature of 450 °C, the ML VSe_2 film shows a 1D discommensurate CDW, as shown in figure 7(d). At high growth temperature, BL VSe_2 are distorted 1T phase (figure 7(e)). Besides, another CDW phase is observed in ML VSe_2 showing $\sqrt{3}\times2$ and $\sqrt{3}\times\sqrt{7}$ periodicities (figure 7(f)) [119]. Kim *et al* considered that the modulations were caused by strong lattice distortions. In contrast to the 1T structure in ML VSe_2, 1T′ structure is stable in BL VSe_2 [120]. Subsequently, Kim *et al* systematically investigated the lattice dynamics in BL 1T′-VSe_2 on EG/SiC and they demonstrated that tunneling current played an important role in lattice dynamics in BL VSe_2 [121]. Kim *et al* also investigated the relationship between multiple CDW phases in ML VSe_2 and the thickness of graphene with STM and ARPES [122]. They found that ML VSe_2 films on SLG and BLG displayed different topographic modulations. They observed$\sqrt{3}\times2$ and $\sqrt{3}\times\sqrt{7}$ CDW in ML VSe2/BLG, but the modulation of 4 × 1 CDW dominated in ML VSe2/SLG. The different topographic modulations arise from different interfaces between the VSe2 and substrates. The weakly coupled interface between ML VSe_2 and SLG substrate might facilitate preserving the 4 × 1 CDW in topography. They demonstrated that SLG and BLG substrates played important roles in studying the CDW phase in TMDs materials.

3.5. $PdSe_2$

The model of $PdSe_2$ is shown in figure 8(a) [123], which is also typical sandwich structure. The electronic structure of $PdSe_2$ is strongly dependent on the number of layers. Singh *et al* demonstrated that bulk $PdSe_2$ was an indirect semiconductor with the bandgap of 0.03 eV and ML $PdSe_2$ was a direct semiconductor with the bandgap of 1.43 eV [124]. Meanwhile, few-layer $PdSe_2$ also has a high electron field-effect mobility, which is beneficial to transistor applications [125, 126], and displays high performance in optoelectronic devices. Besides, due to its broad absorption spectrum (from the visible to ultraviolet regions), $PdSe_2$ has great application potential in solar cell and photovoltaic device [127, 128]. In addition, $PdSe_2$ is relatively stable in air, which is favorable to 2D materials in practical applications [129].

In 2018, Gao *et al* fabricated BL $PdSe_2$ films on EG/SiC surface and the topographic characteristics and electronic properties of the $PdSe_2$ layers were studied by STM/STS [130]. The STM topographic images of $PdSe_2$ is shown in figures 8(b) and (c). They found that the height of the $PdSe_2$ island was about 7.8 Å, indicating that the islands consisted of BL $PdSe_2$. Moreover, the topmost Se atoms were marked white zigzag line in figure 8(c). Through theoretical calculation, they found that BL $PdSe_2$ was indirect bandgap

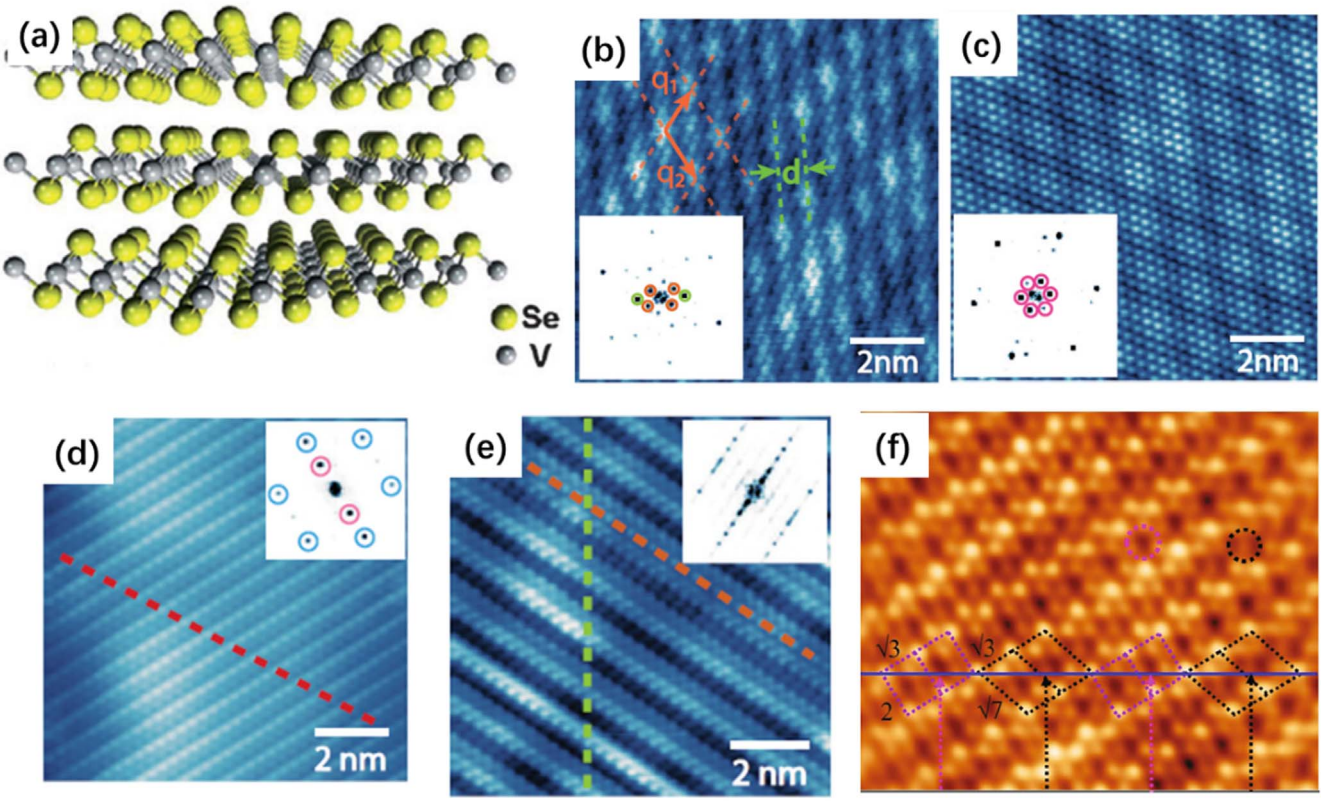

Figure 7. (a) The structure of VSe_2. [117] John Wiley & Sons. Copyright © 2013 WILEY-VCH Verlag GmbH & Co. KGaA, Weinheim. (b) and (c) Morphologies of the SL and BL VSe_2 grow in 200 °C. (d) and (e) Morphologies of SL and BL VSe_2 grow in 450 °C, respectively. Insets: corresponding 2D fast Fourier transform images. Reprinted figure with permission from [118], Copyright (2020) by the American Physical Society. (f) Morphologies of ML VSe_2. Reproduced from [119], with permission from Springer Nature.

semiconductor and the bandgap was 0.94 eV (figure 8(d)). The dI/dV curve of BL $PdSe_2$ on graphene was shown in figure 8(e) and they found that the the bandgap was 1.15 eV, which was larger than the calculated value. Due to excitonic effects in 2D semiconductor [131], Xiao *et al* found that the bandgap of exfoliated BL $PdSe_2$ films characterized by optical spectroscopy was smaller than STS results [129].

Gao *et al* also found $PdSe_2$ films can grow continuously across BLG-MLG steps and corresponding STM image and STS spectra were shown in figures 8(f) and (g), respectively. The dI/dV spectra of $PdSe_2$ films on BLG and MLG showed a distinct shift of 0.2 eV, and they thought that it may be due to the doping effect of SiC substrate, which was similar to [76]. Moreover, the result was further supported by the dI/dV mapping. Besides 2D $PdSe_2$ islands, they also acquired the STM image of a BL $PdSe_2$ nanoribbon on $PdSe_2$ island and the orientation of the nanoribbon was as same as underling $PdSe_2$ island, indicating that $PdSe_2$ nanoribbon epitaxial grew at 2D $PdSe_2$ substrate. In addition, Gao *et al* also synthesized ML Pd_2Se_3 films on EG/SiC by a two-step thermal-annealing process. The STM image is shown in figure 8(h) [132]. Firstly, they fabricated the BL $PdSe_2$ films in the selenium-rich atmosphere. Then, large scale ML Pd_2Se_3 islands could be synthesized by annealing the $PdSe_2$ films in a selenium-deficient atmosphere. The high resolution STM image of Pd_2Se_3 film is shown in figure 8(h).

3.6. $MoTe_2$

Among VI B group TMDs, the energy between 2H-$MoTe_2$ and 1T′-$MoTe_2$ is the most similar [133]. Both high quality thin films can be obtained [134, 135]. 2H-$MoTe_2$ is a semiconductor with a very small bandgap [136], and few-layer $MoTe_2$ can be fabricated as ambipolar field effect transistor. Therefore, homogeneous *p–n* junctions can be constructed by electrostatic doping or surface doping, so as to produce high-performance logic circuits, photodetectors and light-emitting diodes [137–139]. 1T′-$MoTe_2$ is semimetallic, and it has been predicated to be fine material for realizing QSH effect [140].

CVD has been used to prepare the 1T′-$MoTe_2$ films [141]. Up to now, despite the unremitting efforts of researchers, the growth of ML 1T′-$MoTe_2$ films by MBE remains a challenge due to existence of the stable 2H phase in the as-grown 1T′-$MoTe_2$ films [142]. Sporken *et al* have reported the dependence of $MoTe_2$ composition on the growth temperature by MBE on EG/6H-SiC substrates and have found the appropriate temperature for growing the $MoTe_2$ films [33]. They demonstrated that the substrate temperature would affect the crystalline quality of $MoTe_2$. They prepared six samples at different substrate temperatures ranging from 130 °C to 320 °C. As a result, they found that the sample with a substrate temperature of 250 °C had a smoother surface than other samples. They also found the co-existence of the 1T′ phase and 2H phase on the graphene

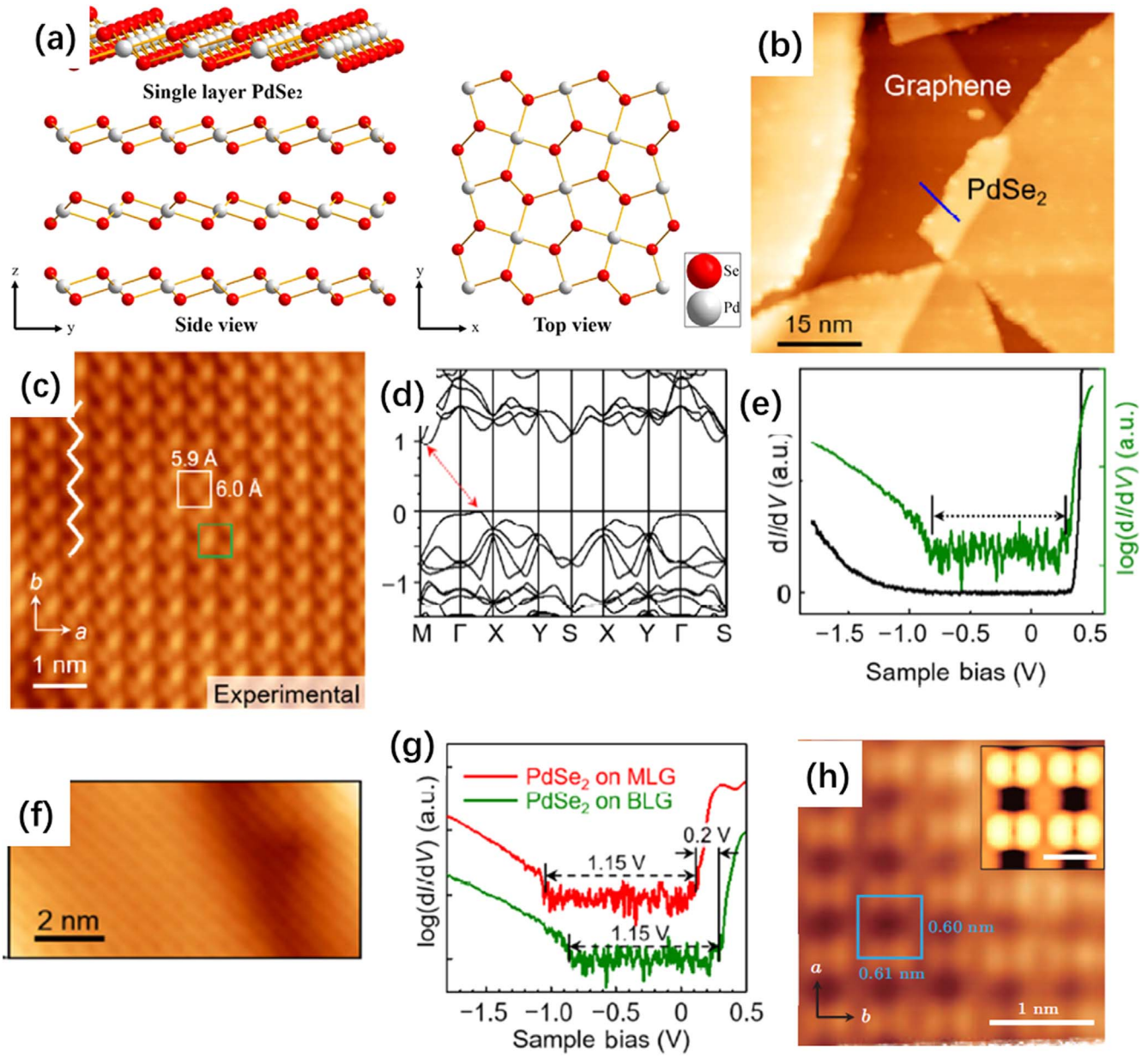

Figure 8. (a) The mold of $PdSe_2$. Reproduced from [123]. © IOP Publishing Ltd. All rights reserved. (b), (c) The STM images of $PdSe_2$ films on EG/SiC surface. (d), (e) Calculated band structure and STS date of BL $PdSe_2$. (f) STM image reveals the continuity of the $PdSe_2$ across the BLG and MLG steps. (g) STS data of the $PdSe_2$ island on BLG and MLG. Reproduced from [130], with permission from Springer Nature. (h) The STM image of Pd_2Se_3. Reproduced from [132]. © Chinese Physical Society. All rights reserved.

surface (figure 9(a)). Ball-and-stick models of the 2H-$MoTe_2$ and 1T′-$MoTe_2$ are shown in figures 9(b) and (c), respectively [143]. Meanwhile, Zhang *et al* utilized STM/STS to investigate the morphologies and electronic properties of lateral heterophase homojunctions in epitaxial 2H-$MoTe_2$ and 1T′-$MoTe_2$ films on EG surface [143]. 2H- and 1T′-phase edges can form continuous interfaces and larger $MoTe_2$ islands can be observed in figures 9(d) and (e). They further acquired the dI/dV spectra of the point A ∼ G in figure 9(e), as shown in figure 9(f). At point A, the dI/dV curve is V-type, but it turns into U-type at point G, indicating the structure can transform from semimetallic 1T′ phase to semiconducting 2H phase. This study reveals that $MoTe_2$ lateral homojunctions can be fabricated on graphene, which will display great applications in novel phase patterning devices.

Since the energy of 2H and 1 T′ phases is close, it is difficult to fabricate single phase 2H-$MoTe_2$ films. Adjusting the growth conditions instead of increasing growth steps is the best way to get a single crystallographic phase, since too many growth processes will destroy the crystalline quality [144, 145]. Recently. Sporken *et al* fabricated only 2H-$MoTe_2$ phase via MBE with a multi-step process [146] and uniform 2H-$MoTe_2$ films could be obtained in figure 9(g). Two different Moiré patterns can be observed in this ML 2H-$MoTe_2$ as shown in figure 9(h). On the BLG surface two different Moiré patterns have been also observed [147]. As a

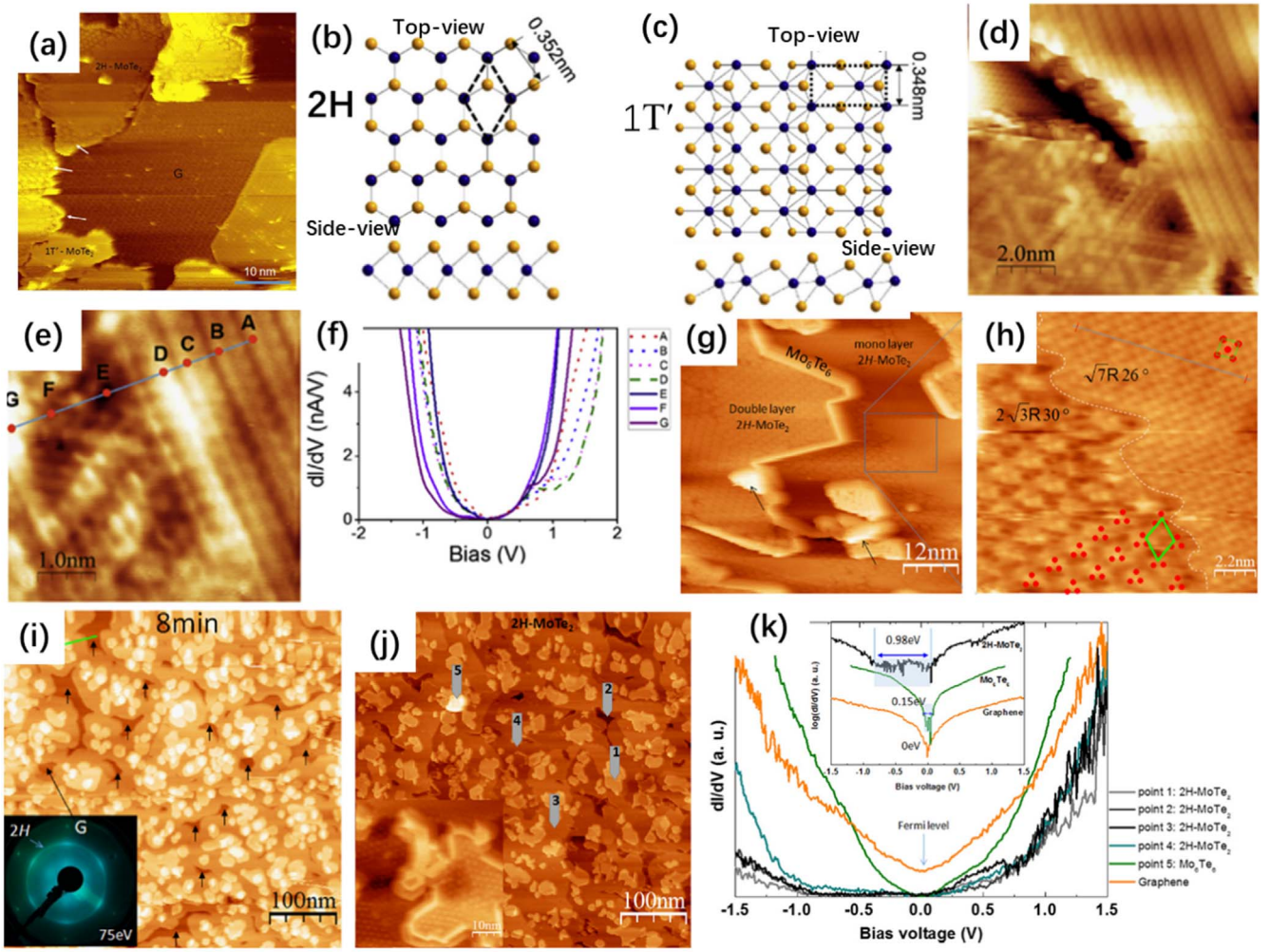

Figure 9. (a) An STM image of $MoTe_2$ on BLG deposited at 250 °C. Reproduced from [33]. © IOP Publishing Ltd. All rights reserved. (b)–(c) are the ball-and-stick model of 2H and 1T′-$MoTe_2$. (d)–(f) STM/STS of the 2H-1T′ homojunction. Reprinted from [143], © 2017 Elsevier Ltd. All rights reserved. (g) Morphology of $MoTe_2$ films fabricated in the multi-step process. (h) Two different Moiré patterns in ML 2H-$MoTe_2$. (i) STM images of $MoTe_2$ fabricated in the single-step process. (j), (k) STM/STS data of 2H-$MoTe_2$. Reprinted from [146], © 2020 Elsevier B.V. All rights reserved.

contrast, they fabricated a sample with the same growth time in a single-step process. However, the crystalline quality is poor, the corresponding STM image is shown in figure 9(i). They also prepared a sample with 10 min deposition in the multi-step process, the graphene surface was covered by the 2H-$MoTe_2$ phase (figure 9(j)). STS measurements are performed at points 1–5 in figure 9(j) and corresponding dI/dV curves are shown in figure 9(k). The dI/dV spectra of graphene and Mo_6Te_6 are 'V'-type, because they are semimetallic. Other dI/dV curves are 'U' shape, indicating 2H-$MoTe_2$ is semiconducting. The bandgap of 2H-$MoTe_2$ is ~0.98 eV, which is consistent with the previous report [146]. Sporken *et al* also demonstrated that 2H-$MoTe_2$ films could recover to high quality surface after exposure to air under a dry nitrogen box [148]. Zhou *et al* successfully prepared 1T′-$MoTe_2$ films on BLG/6H-SiC [149]. Moreover, they demonstrated that 1T′-$MoTe_2$ film was a metal. In addition, in another report, Sporken *et al* also found three different Moiré patterns in 1H-$MoTe_2$ films by using appropriate scanning conditions [150]. The atomically clean interface between graphene and $MoTe_2$ permits the electronic coupling between the adjacent layers and the appearance of a high variety of Moiré patterns. This result revealed the complex electronic coupling of the $MoTe_2$/graphene heterostructure.

3.7. WTe_2

The model of ML 1T′-WTe_2 is shown in figure 10(a), it is a typical sandwich structure [151]. In 2017, Mo *et al* obtained ML 1T′-WTe_2 films by MBE on the EG/SiC substrate (figure 10(b)) [152]. Comparing with STS and ARPES results, they confirmed that the bandgap of ML 1T′-WTe_2 was 55 meV (figure 10(c)). The STS data was acquired at a point far away from the edge of WTe_2 films, which represented the bulk local DOS. Moreover a QSH insulator of ML 1T′-WTe_2 is first measured by ARPES. STS data acquired at the bulk and the 1T′-WTe_2 edge was very different. The dI/dV spectrum at the 1T′-WTe_2 edge is 'V-shape', but a gap exists in the bulk (figure 10(d)). Besides, they also acquired the spatial profile of the 1T′-WTe_2 edge and bulk states in figure 10(e),

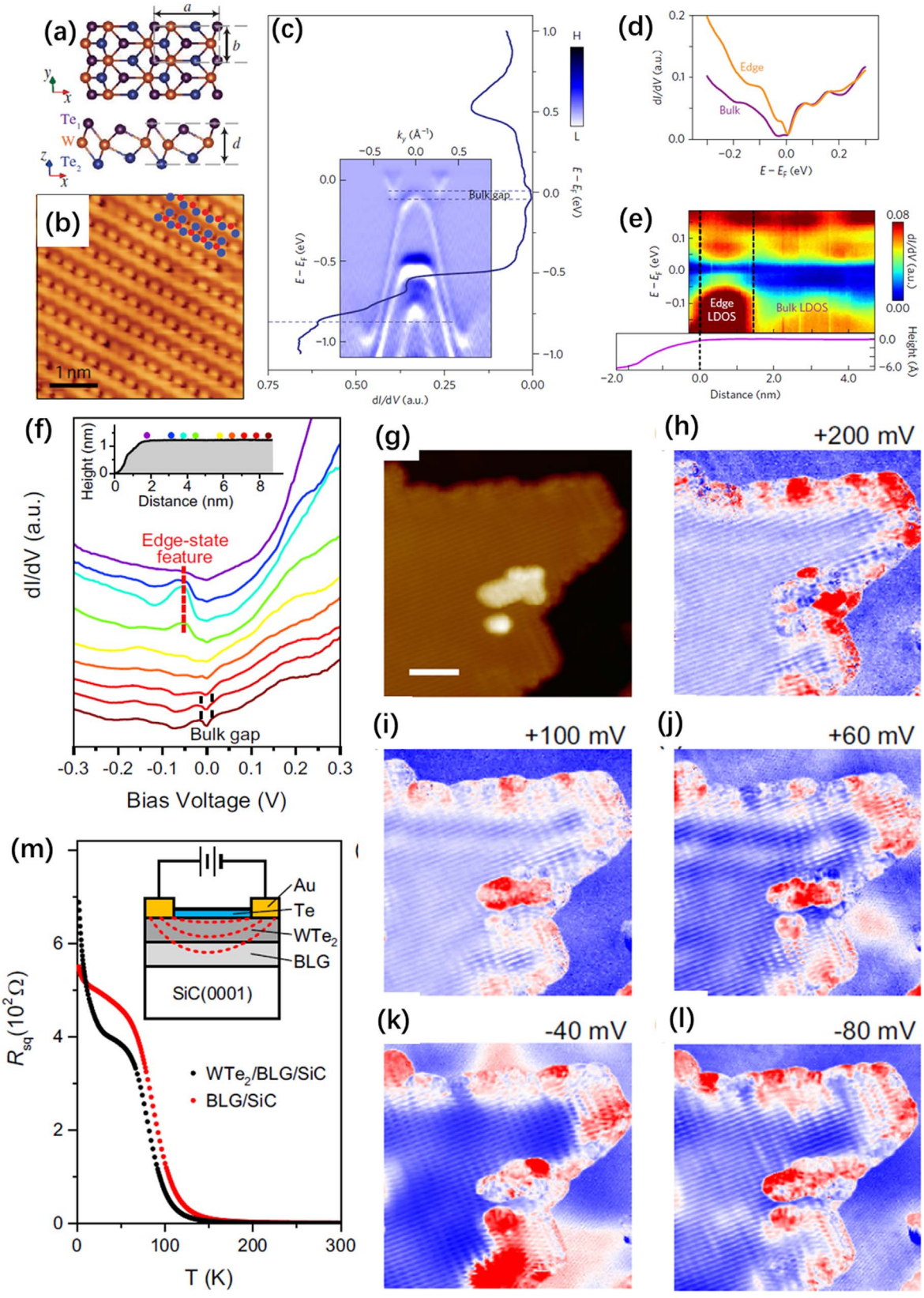

Figure 10. (a) Ball-and-stick model of ML 1T′-WTe_2. Reprinted figure with permission from [151], Copyright (2020) by the American Physical Society. (b) Morphology of 1T′-WTe_2 films. (c) The STS data obtained in the bulk of ML 1T′-WTe_2. The inset is the high-symmetry ARPES cut along the O–Y direction. (d) $\mathrm{d}I/\mathrm{d}V$ spectra of the bulk and the edge of 1T′-WTe_2. (e) Spatial profile of the 1T′-WTe_2 edge and bulk states. Reproduced from [152], with permission from Springer Nature. (f) $\mathrm{d}I/\mathrm{d}V$ data acquired near WTe_2 step edge. (g) and (h)–(l) STM and $\mathrm{d}I/\mathrm{d}V$ maps at different bias. (m) The plot of square resistance versus temperature. Reprinted figure with permission from [154], Copyright (2017) by the American Physical Society.

where a gap in bulk and metallic edges could be observed. In contrast to the ARPES result (figure 10(c)), they considered that a bandgap of bulk was 55 meV, which is in agreement with theoretical predictions [106]. Recently, Cobden *et al* demonstrated that conducting edge channels were observed in exfoliated 1T′-WTe_2 [153]. Li *et al* obtained nearly free-standing SL 1T′-WTe_2 on EG/SiC by MBE [154]. They confirmed that the topological edge states existed in the edge of SL WTe_2 islands. The dI/dV data were acquired across the WTe_2 step edge as shown in figure 10(f). They found that the peak only appeared near the step edge in the range of 5 nm, as indicated by the red dotted line. Moreover, due to the enhancement of the dI/dV intensities along the step edges changes subtly, they considered that the edge states were stable to the weak perturbations at the steps. A topographic image and corresponding dI/dV maps are acquired at different bias, in figures 10(g) and (h)–(l), respectively. The edge states are always at the edge of the WTe_2 steps, as marked by the enhanced dI/dV intensity. They also measured temperature-dependent resistance over the SL WTe_2 films and the corresponding relationship was shown in figure 10(m). Moreover, they also confirmed that the SL WTe_2 films act as an insulator below 30 K.

2D 1 T′-WTe_2 also has strong electron correlation [155]. Song *et al* reveled that there was a weak pseudogap suppression in the DOS [156], when the ML WTe_2 films were doped so that the Fermi level was located in the CB. Zhao *et al* demonstrated that the strain could be tuned by using the distorted graphene as substrate, which is fabricated by overheating the SiC sample [151]. They found that the band structures of the ML 1T′-WTe_2 could be regulated by in-plane strain and the phase transition can be tuned from a semimetal to an insulator.

3.8. $PdTe_2$

$PdTe_2$ is a typical 1T structure [157, 158]. In particular, $PdTe_2$ is a 2D layered material with low temperature superconductivity, which makes it an interesting material for condensed matter explorations. Schematic structure of bulk $PdTe_2$ is shown in figure 11(a). In 2018, Gao *et al* reported the epitaxial growth of large area $PdTe_2$ materials on EG/SiC substrate via MBE [159]. They obtained atomically resolved STM image of $PdTe_2$ films (figure 11(b)). Furthermore, they carried out the air exposure measurements and proved the chemical stability of $PdTe_2$. They firstly exposed the epitaxial $PdTe_2$ sample to air more than 5 h. Then, the sample was annealed at 450 K in UHV to desorb the physisorbed species. High quality $PdTe_2$ films can also be obtained and the STM images are shown in figure 11(c) (large-area) and 11(d) (atomically resolved). The $PdTe_2$ films can construct antimonene/$PdTe_2$ heterojunctions for future applications in optoelectronic devices.

3.9. Other transition metal dichalcogenides

Other TMDs have been successfully grown on EG/SiC by MBE and measured by STM include $TiSe_2$, Cu_2Te, $CrTe_2$, NbS_2, TaS_2 and FeS_2, and so on. In one report, Peng *et al* have grown $TiSe_2$ films on EG/SiC via MBE and have identified two dominant types of Se vacancy and interstitial defects by STM measurements [160]. In another report, Qian *et al* have recently fabricated ML Cu_2Te films on EG/SiC via MBE with excellent air stability [161]. In 2021, Zhang *et al* have shown the growth of $CrTe_2$ films by MBE, for the first time and have observed intrinsic ferromagnetism in $CrTe_2$ films [162]. In addition, Lin *et al* have revealed that monolayer NbS_2, TaS_2, and FeS films can be synthesized on EG/SiC via MBE by using FeS as the sulfur source and CDW patterns can be observed in monolayer NbS_2, TaS_2 [163]. Thus, this work provides a method to fabricate 2D materials by using FeS as the sulfur source, which can be useful for growing 2D sulfides in the future.

4. Summary and future outlook

In this paper, the research progress of 2D layered materials on EG/SiC by MBE is reviewed, including monoelemental (e.g. silicene, bismuthene, tellurene) and TMDs. The topographic characteristics and the electronic properties of these 2D layered materials are measured by STM/STS are summarized. Through the precise control of MBE, 2D layered materials on EG/SiC substrate can grow layer by layer after nucleation and some important naturally non-existent or unstable 2D layered materials can be fabricated. By varying the heating parameters of the evaporation source and the time during the epitaxial process, the researchers can control the specific number of 2D layered materials layers on EG/SiC. Thus, MBE-grown 2D materials generally have high crystal quality and few defects. However, sometimes the localized characterization of STM/STS makes them not a best means to analyze crystal quality. Even a certain number of defects are observed in the STM images, these defects are insignificant on the entire 2D materials at the macro level. To further explore this question, it is necessary to combine with some other characterization methods, such as transmission electron microscopy, high energy resolution analysis deep level transient spectroscopy and so on. For MBE, precise doping is one of the outstanding advantages, which can give 2D materials entirely new properties. Combined with STM/STS, the atomic and electronic structure of doping atoms can be obtained. At present, there is not much research on the MBE-grown doping of 2D materials on SiC/EG. Considering the abundance of doping atoms, this is a field to further explored.

Although breakthroughs or gains have been obtained on the fabrication of 2D layered materials on EG/SiC by MBE, there are a lot of questions and problems which have not been solved yet. For instance, some important 2D layered materials have not been obtained on EG/SiC surface by MBE, such as MoS_2 and many important monoelemental 2D layered materials. Moreover, the fabrication of monolayer alloys with three elements or more by MBE is rare. In addition, the precise control of MBE also means the slow epitaxial speed and only one substrate can be grown in an MBE device,

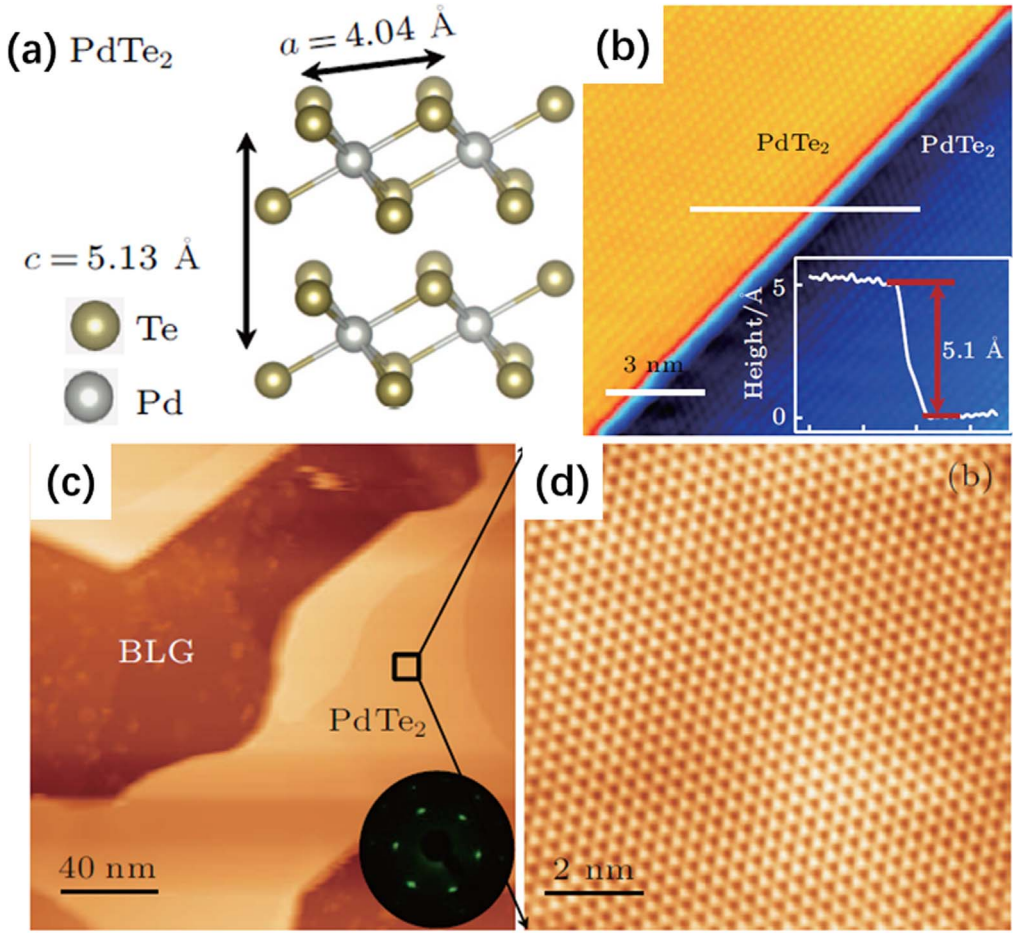

Figure 11. (a) Schematic illustration of $PdTe_2$. (b) STM image of $PdTe_2$. Inset: height profile along the white line. (c)–(d) STM image of $PdTe_2$ after being exposed to air. Insets: the LEED pattern of $PdTe_2$ on EG/SiC after being exposed to air. Reproduced from [159].

which involves the economic practicability in actual production.

Acknowledgments

This work is supported by 'Pioneer' and 'Leading Goose' R&D Program of Zhejiang (Grant No. 2022C01021) and Natural Science Foundation of China (Grant Nos. 91964107 and U20A20209). Partial support from Natural Science Foundation of China for Innovative Research Groups (Grant No. 61721005) is acknowledged.

Data availability statement

No new data were created or analysed in this study.

ORCID iDs

Yiqiang Zhang https://orcid.org/0000-0002-2437-925X
Xiaodong Pi https://orcid.org/0000-0002-4233-6181

References

[1] Zhou D, Li H, Si N, Li H, Fuchs H and Niu T 2021 Epitaxial growth of main group monoelemental 2D materials *Adv. Funct. Mater.* **31** 2006997
[2] Mas-Ballesté R, Gómez-Navarro C, Gómez-Herrero J and Zamora F 2011 2D materials: to graphene and beyond *Nanoscale* **3** 20–30
[3] Xu Y and Shi G 2010 Assembly of chemically modified graphene: methods and applications *J. Mater. Chem.* **21** 3311–23
[4] Wu L *et al* 2020 InSe/hBN/graphite heterostructure for high-performance 2D electronics and flexible electronics *Nano Res.* **13** 1127–32
[5] Zhu C, Du D and Lin Y 2015 Graphene and graphene-like 2D materials for optical biosensing and bioimaging: a review *2D Mater.* **2** 032004
[6] Novoselov K S, Mishchenko A, Carvalho A and Castro Neto A H 2016 2D materials and van der Waals heterostructures *Science* **353** aac9439
[7] Li H, Lu G, Wang Y, Yin Z, Cong C, He Q, Wang L, Ding F, Yu T and Zhang H 2013 Mechanical exfoliation and characterization of single- and few-layer nanosheets of WSe_2, TaS_2, and $TaSe_2$ *Small* **9** 1974–82
[8] Coleman J N *et al* 2011 Two-dimensional nanosheets produced by liquid exfoliation of layered materials *Science* **331** 568–71

[9] Splendiani A, Sun L, Zhang Y, Li T, Kim J, Chim C Y, Galli G and Wang F 2010 Emerging photoluminescence in monolayer MoS_2 *Nano Lett.* **10** 1271–5

[10] Pham T T, Castelino R, Felten A and Sporken R 2020 Preparation of single phase 2H-$MoTe_2$ films by molecular beam epitaxy *Appl. Surf. Sci.* **219** 238–48

[11] Dumcenco D *et al* 2015 Large-area epitaxial monolayer MoS_2 *ACS Nano* **9** 4611–20

[12] Feng B, Ding Z, Meng S, Yao Y, He X, Cheng P, Chen L and Wu K 2012 Evidence of silicene in honeycomb structures of silicon on Ag(111) *Nano Lett.* **12** 3507–11

[13] Reis F, Li G, Dudy L, Bauernfeind M, Glass S, Hanke W, Thomale R, Schäfer J and Claessen R 2017 Bismuthene on a SiC substrate: a candidate for a high-temperature quantum spin Hall material *Science* **357** 287–90

[14] Zhang J L *et al* 2016 Epitaxial growth of single layer blue phosphorus: a new phase of two-dimensional phosphorus *Nano Lett.* **16** 4903–8

[15] Li L, Lu S Z, Pan J, Qin Z, Wang Y Q, Wang Y, Cao G Y, Du S and Gao H J 2014 Buckled germanene formation on Pt(111) *Adv. Mater.* **26** 4820–4

[16] Deng J *et al* 2018 Epitaxial growth of ultraflat stanene with topological band inversion *Nat. Mater.* **17** 1081–6

[17] Schwarz M *et al* 2017 Corrugation in the weakly interacting hexagonal-BN/Cu(111) system: structure determination by combining noncontact atomic force microscopy and x-ray standing waves *ACS Nano* **11** 9151–61

[18] Fleurence A, Friedlein R, Ozaki T, Kawai H, Wang Y and Yamada-Takamura Y 2012 Experimental evidence for epitaxial silicene on diboride thin films *Phys. Rev. Lett.* **108** 245501

[19] Wang Y Y, Li J, Xiong J, Pan Y, Ye M, Guo Y, Zhang H, Quhe R and Lu J 2016 Does the Dirac cone of germanene exist on metal substrates? *Phys. Chem. Chem. Phys.* **18** 19451–6

[20] Chen M X and Weinert M 2014 Revealing the substrate origin of the linear dispersion of silicene/Ag(111) *Nano Lett.* **14** 5189–93

[21] Acun A, Poelsema B, Zandvliet H J W and Gastel R V 2013 The instability of silicene on Ag(111) *Appl. Phys. Lett.* **103** 263119

[22] Stankovich S, Dikin D A, Dommett G H B, Kohlhaas K M, Zimney E J, Stach E A, Piner R D, Nguyen S T and Ruoff R S 2006 Graphene-based composite materials *Nature* **442** 282–6

[23] Kim K S, Zhao Y, Jang H, Lee S Y, Kim J M, Kim K S, Ahn J H, Kim P, Choi J Y and Hong B H 2009 Large-scale pattern growth of graphene films for stretchable transparent electrodes *Nature* **457** 706–10

[24] Yang H, Heo J, Park S, Song H J, Seo D H, Byun K E, Kim P, Yoo I, Chung H J and Kim K 2012 Graphene barristor, a triode device with a gate-controlled Schottky barrier *Science* **336** 1140–3

[25] Li Z, Wu S, Lv W, Shao J J, Kang F and Yang Q H 2016 Graphene emerges as a versatile template for materials preparation *Small* **12** 2674–88

[26] Lasek K, Li J, Kolekar S, Coelho P M, Guo L, Zhang M, Wang Z and Batzill M 2021 Synthesis and characterization of 2D transition metal dichalcogenides: recent progress from a vacuum surface science perspective *Surf. Sci. Rep.* **76** 100523

[27] Geim A K and Novoselov K S 2007 The rise of graphene *Nat. Mater.* **6** 183–91

[28] Berger C *et al* 2006 Electronic confinement and coherence in patterned epitaxial graphene *Science* **312** 1191

[29] Kim J *et al* 2014 Principle of direct van der Waals epitaxy of single-crystalline films on epitaxial graphene *Nat. Commun.* **5** 4836

[30] Chang K *et al* 2016 Discovery of robust in-plane ferroelectricity in atomic-thick SnTe *Science* **353** 274–8

[31] Li C H, Erve J V, Robinson J T, Liu Y, Li L and Jonker B T 2014 Electrical detection of charge-current-induced spin polarization due to spin-momentum locking in Bi_2Se_3 *Nat. Nanotech.* **9** 218–24

[32] Yu Y, Wang G, Tan Y, Wu N, Zhang X A and Qin S 2018 Phase-controlled growth of one-dimensional Mo_6Te_6 nanowires and two-dimensional $MoTe_2$ ultrathin films heterostructures *Nano Lett.* **18** 675–81

[33] Castelino R, Pham T T, Felten A and Sporken R 2020 Substrate temperature dependence of the crystalline quality for the synthesis of pure-phase $MoTe_2$ on graphene/6H-SiC (0001) by molecular beam epitaxy *Nanotechnology* **31** 115702

[34] Chen W *et al* 2019 Growth and thermo-driven crystalline phase transition of metastable monolayer 1T′-WSe2 thin film *Sci. Rep.* **9** 2685

[35] Ryu H *et al* 2018 Persistent charge-density-wave order in single-layer $TaSe_2$ *Nano Lett.* **18** 689–94

[36] Chen Y, Liu L, Song X, Yang H, Hang Z, Zhang T, Yang H, Gao H J and Wang Y 2022 Twisted charge-density-wave patterns in bilayer 2D crystals and modulated electronic states *2D Mater.* **9** 014007

[37] Liu L *et al* 2021 Direct identification of Mott Hubbard band pattern beyond charge density wave superlattice in monolayer 1T-$NbSe_2$ *Nat. Commun.* **12** 1798

[38] Pielic B, Novko D, Rakic S, Cai J, Petrovic M, Ohmann R, Vujicic N, Basletic M, Busse C and Kralj M 2021 Electronic structure of quasi-freestanding WS_2/MoS_2 heterostructure *ACS Appl. Mater. Interfaces* **13** 50552–63

[39] Qiu Z *et al* 2021 Visualizing atomic structure and magnetism of 2D magnetic insulators via tunneling through graphene *Nat. Commun.* **12** 70

[40] Vancsó P, Mayer A, Nemes-Incze P and Nemes-Incze G 2021 Wave packet dynamical simulation of quasiparticle interferences in 2D materials *Appl. Sci.* **11** 4730

[41] Yuan Y, Yang X, Peng L, Wang Z J, Li J, Yi C J, Xian J J, Shi Y G and F Y S 2018 Quasiparticle interference of Fermi arc states in the type-II Weyl semimetal candidate WTe_2 *Phys. Rev.* B **97** 165435

[42] Kwon H, Jeong T, Appalakondaiah S, Oh Y, Jeon I, Min H, Park S, Song Y J, Hwang E and Hwang S 2020 Quasiparticle interference and impurity resonances on WTe_2 *Nano Res.* **13** 2534–40

[43] Zhang C *et al* 2016 Visualizing band offsets and edge states in bilayer–monolayer transition metal dichalcogenides lateral heterojunction *Nat. Commun.* **7** 10349

[44] Wang N, Gao H, Liu Y J, Zhao J X, Cai Q H and Wang X Z 2015 Asymmetric functionalization as a promising route to open the band gap of silicene: a theoretical prediction *Physica* E **73** 21–6

[45] Cahangirov S, Topsakal M, Aktürk E , S, ahin H and Ciraci S 2009 Two- and one-dimensional honeycomb structures of silicon and germanium *Phys. Rev. Lett.* **102** 236804

[46] Ezawa M 2012 Valley-polarized metals and quantum anomalous hall effect in silicene *Phys. Rev. Lett.* **109** 055502

[47] Liu C C, Feng W and Yao Y 2011 Quantum spin hall effect in silicene and two-dimensional germanium *Phys. Rev. Lett.* **107** 076802

[48] Meng L *et al* 2013 Buckled silicene formation on Ir(111) *Nano Lett.* **13** 685–90

[49] Satta M, Colonna S, Flammini R, Cricenti A and Ronci F 2015 Silicon reactivity at the Ag(111) surface *Phys. Rev. Lett.* **115** 026102

[50] Sone J, Yamagami T, Nakatsuji K and Hirayama H 2016 Si growth at graphene surfaces on 6H-SiC(0001) substrates *Jpn. J. Appl. Phys.* **55** 035502

[51] Berbezier I, Michon A, Castrucci P, Scarselli M, Salvato M, Scagliotti M and Crescenzi M D 2019 Silicene nanostructures grown on graphene covered SiC (0001) substrate *Int. J. Nanosci.* **18** 1940039

[52] Jabra Z B *et al* 2022 Van der Waals heteroepitaxy of air-stable quasi-free-standing silicene layers on CVD epitaxial graphene/6H-SiC *ACS Nano* **16** 5920–31

[53] Yao M Y, Zhu F, Han C Q, Guan D D, Liu C, Qian D and Jia J F 2016 Topologically nontrivial bismuth(111) thin films *Sci. Rep.* **6** 21326

[54] Chen H H, Su S H, Chang S L, Cheng B Y, Chong C W, Huang J C A and Lin M F 2015 Long-range interactions of bismuth growth on monolayer epitaxial graphene at room Temperature *Carbon* **93** 1180–6

[55] Ast C R and Höchst H 2001 Fermi surface of Bi(111) measured by photoemission spectroscopy *Phys. Rev. Lett.* **87** 177602

[56] Yang F Y, Liu K, Hong K, Reich D H, Searson P C and Chien C L 1999 Large magnetoresistance of electrodeposited single-crystal bismuth thin films *Science* **284** 11335–7

[57] Weitzel B and Micklitz H 1991 Superconductivity in granular systems built from well-defined rhombohedral Bi clusters: evidence for Bi-surface superconductivity *Phys. Rev. Lett.* **66** 385–8

[58] Hoffman C A, Meyer J R and Bartoli F J 1993 Semimetal-to-semiconductor transition in bismuth thin films *Phys. Rev.* B **104** 045432

[59] Ge J L, Wu T R, Gao M, Bai Z B, Cao L, Wang X, Qin Y Y and Song F Q 2017 Weak localization of bismuth cluster-decorated graphene and its spin–orbit interaction *Front. Phys.* **12** 127210

[60] Kowalczyk P J, Mahapatra O, McCarthy D N, Kozlowski W, Klusek Z and Brown S A 2011 STM and XPS investigations of bismuth islands on HOPG *Surf. Sci.* **605** 659–67

[61] Hirahara T, Nagao T, Matsuda I, Bihlmayer G, Chulkov E V, Koroteev Y M, Echenique P M, Saito M and Hasegawa S 2006 Role of spin–orbit coupling and hybridization effects in the electronic structure of ultrathin Bi films *Phys. Rev. Lett.* **97** 146803

[62] Yang F *et al* 2012 Spatial and energy distribution of topological edge states in single Bi(111) bilayer *Phys. Rev. Lett.* **109** 016801

[63] Zhang H L, Chen W, Wang X S, Yuhara J and Wee A T S 2009 Growth of well-aligned Bi nanowire on Ag(111) *Appl. Surf. Sci.* **256** 460–4

[64] Huang H, Wong S L, Wang Y, Sun J T, Gao X and Wee A T S 2014 Scanning tunneling microscope and photoemission spectroscopy investigations of bismuth on epitaxial graphene on SiC(0001) *J. Phys. Chem.* C **118** 24995–9

[65] Hu T, Hui X, Zhang X, Liu X, Ma D, Wei R, Xu K and Ma F 2018 Nanostructured Bi grown on epitaxial graphene/SiC *J. Phys. Chem. Lett.* **9** 5679–84

[66] Hu T, Ma D, Fang Q, Zhang P, Liu X, Wei R, Pan Y, Xu K and Ma F 2019 Bismuth mediated defect engineering of epitaxial graphene on SiC(0001) *Carbon* **146** 313–9

[67] Apte A *et al* 2018 Polytypism in ultrathin tellurium *2D Mater.* **6** 015013

[68] Amani M, Tan C, Zhang G, Zhao C, Bullock J, Song X, Kim H, Shrestha V R, Gao Y and Crozier K B 2018 Solution-synthesized high-mobility tellurium nanoflakes for short-wave infrared photodetectors *ACS Nano* **12** 7253–63

[69] Zhao C *et al* 2020 Evaporated tellurium thin films for p-type field-effect transistors and circuits *Nat. Nanotechnol.* **15** 53–8

[70] Gan X *et al* 2020 Giant and anisotropic nonlinear optical responses of 1D van der Waals material tellurium *Adv. Opt. Mater.* **8** 015013

[71] Hawley C J, Beatty B R, Chen G and Spanier J 2012 Shape-controlled vapor-transport growth of tellurium nanowires *Cryst. Growth Des.* **12** 2789–93

[72] Tai G, Zhou B and Guo W 2008 Structural characterization and thermoelectric transport properties of uniform single-crystalline lead telluride nanowires *J. Phys. Chem.* C **112** 11314–8

[73] Wang Q, Safdar M, Xu K, Mirza M, Wang Z and He J 2014 Van der Waals epitaxy and photoresponse of hexagonal tellurium nanoplates on flexible mica sheets *ACS Nano* **8** 7497–505

[74] Huang X, Guan J, Lin Z, Liu B, Xing S, Wang W and Guo J 2017 Epitaxial growth and band structure of Te film on graphene *Nano Lett.* **17** 4619–23

[75] Miao G, Qiao J, Huang X, Liu B, Zhong W, Wang W, Ji W and Guo J 2021 Quasiperiodic modulation of electronic states at edges of tellurium nanoribbons on graphene/6H-SiC(0001) *Phys. Rev.* B **103** 235421

[76] Huang X, Liu B, Guan J, Miao G, Lin Z, An Q, Zhu X, Wang W and Guo J 2018 Realization of in-plane *p–n* junctions with continuous lattice of a homogeneous material *Adv. Mater.* **30** 1802065

[77] Radisavljevic B, Radenovic A, Brivio J, Giacometti V and Kis A 2011 Single-layer MoS_2 transistors *Nat. Nanotechnol.* **6** 147–50

[78] Chhowalla M, Shin H S, Eda G, Li L J, Loh K P and Zhang H 2013 The chemistry of two-dimensional layered transition metal dichalcogenide nanosheets *Nat. Chem.* **5** 263–75

[79] Mak K F, Lee C, Hone J, Shan and Heinz T F 2010 Atomically thin MoS_2: a new direct-gap semiconductor *Phys. Rev. Lett.* **105** 1802065

[80] Bollinger M V, Jacobsen K W and Nørskov J K 2003 Atomic and electronic structure of MoS_2 nanoparticles *Phys. Rev.* B **67** 085410

[81] Li T and Galli G 2007 Electronic properties of MoS_2 nanoparticles *J. Phys. Chem.* C **111** 16192–6

[82] Vishwanath S *et al* 2015 Comprehensive structural and optical characterization of MBE grown $MoSe_2$ on graphite, CaF_2 and graphene *2D Mater.* **2** 024007

[83] Xia J, Huang X, Liu L Z, Wang M, Wang L, Huang B, Zhu D D, Li J J, Gu C Z and Meng X M 2014 CVD synthesis of large-area, highly crystalline $MoSe_2$ atomic layers on diverse substrates and application to photodetectors *Nanoscale* **6** 8949–55

[84] Jin Y, Keum D H, An S J, Kim J, Lee H S and Lee Y H 2015 A Van Der Waals homojunction: ideal *p–n* diode behavior in MoSe *Adv. Mater.* **27** 5534–40

[85] Choi W, Choudhary N, Han G H, Park J, Akinwande D and Lee Y H 2017 Recent development of two-dimensional transition metal dichalcogenides and their applications *Mater. Today* **20** 116–30

[86] Ugeda M M *et al* 2014 Giant bandgap renormalization and excitonic effects in a monolayer transition metal dichalcogenide semiconductor *Nat. Mater.* **13** 1091–5

[87] Zhang Y *et al* 2014 Direct observation of the transition from indirect to direct bandgap in atomically thin epitaxial $MoSe_2$ *Nat. Nanotechnol.* **9** 111–5

[88] Lu J, Bao D L, Qian K, Zhang S, Chen H, Lin X, Du S X and Gao H J 2017 Identifying and visualizing the edge terminations of single-layer $MoSe_2$ Island epitaxially grown on Au(111) *ACS Nano* **11** 1689–95

[89] Barja S *et al* 2016 Charge density wave order in 1D mirror twin boundaries of single-layer $MoSe_2$ *Nat. Phys.* **12** 751–6

[90] Bradley A J *et al* 2015 Probing the role of interlayer coupling and coulomb interactions on electronic structure in few-layer $MoSe_2$ nanostructures *Nano Lett.* **15** 2594–9

[91] Tongay S, Zhou J, Ataca C, Lo K, Matthews T S, Li J, Grossman J C and Wu J 2012 Thermally driven crossover

from indirect toward direct bandgap in 2D semiconductors: $MoSe_2$ versus MoS_2 *Nano Lett.* **12** 5576–80
[92] Eda G, Yamaguchi H, Voiry D, Fujita T, Chen M and Chhowalla M 2011 Photoluminescence from chemically exfoliated MoS_2 *Nano Lett.* **11** 5111–6
[93] Dau M T, Gay M, Felice D D, Vergnaud C, Marty A, Beigné C, Renaud G, Renault O, Mallet P and Quang T L 2018 Beyond van der Waals interaction: the case of $MoSe_2$ epitaxially grown on few-layer graphene *ACS Nano* **12** 2319–31
[94] Rhodes D, Chae S H, Ribeiro-Palau R and Hone J 2019 Disorder in van der Waals heterostructures of 2D materials *Nat. Mater.* **18** 541–9
[95] Lin Z *et al* 2016 Defect engineering of two-dimensional transition-metal dichalcogenides: applications, challenges, and opportunities *2D Mater.* **3** 022002
[96] Janos P *et al* 2018 Spontaneous doping of the basal plane of MoS_2 single layers through oxygen substitution under ambient conditions *Nat. Chem.* **10** 1246–51
[97] Barja S *et al* 2019 Identifying substitutional oxygen as a prolific point defect in monolayer transition metal dichalcogenides *Nat. Commun.* **10** 3382
[98] Zhu Z Y, Cheng Y C and Schwingenschlögl U 2011 Giant spin–orbit-induced spin splitting in two-dimensional transition-metal dichalcogenide semiconductors *Phys. Rev.* B **84** 153402
[99] Xiao D, Liu G B, Feng W, Xu X and Yao W 2012 Coupled spin and valley physics in monolayers of MoS_2 and other group-VI dichalcogenides *Phys. Rev. Lett.* **108** 196802
[100] Huang C, Wu S, Sanchez A M, Peters J J P, Beanland R, Ross J S, Rivera P, Yao W, Cobden D H and Xu X 2014 Lateral heterojunctions within monolayer $MoSe_2$-WSe_2 semiconductors *Nat. Mater.* **13** 1096–101
[101] Liu W, Kang J, Sarkar D, Khatami Y, Jena D and Banerjee K 2013 Role of metal contacts in designing high-performance monolayer n-type WSe_2 field effect transistors *Nano Lett.* **13** 1983–90
[102] Duan X, Wang C, Pan A, Yu R and Duan X 2015 Two-dimensional transition metal dichalcogenides as atomically thin semiconductors: opportunities and challenges *Chem. Soc. Rev.* **44** 8859–76
[103] Liu H J, Jiao L, Xie L, Yang F, Chen J L, Ho W K, Gao C L, Jia J F, Cui X D and Xie M H 2015 Molecular-beam epitaxy of monolayer and bilayer WSe_2: a scanning tunneling microscopy/spectroscopy study and deduction of exciton binding energy *2D Mater.* **2** 034004
[104] Zhang Y *et al* 2016 Electronic structure, surface doping, and optical response in epitaxial WSe2 thin films *Nano Lett.* **16** 2485
[105] Li Y, Qin J K, Xu C Y, Cao J, Sun Z Y, Ma L P, Hu P A, Ren W and Zhen L 2016 Electric field tunable interlayer relaxation process and interlayer coupling in WSe_2/graphene heterostructures *Adv. Funct. Mater.* **26** 4319–28
[106] Chen P, Pai W W, Chan Y H, Sun W L, Xu C Z, Lin D S, Chou M Y, Fedorov A V and Chiang T C 2018 Large quantum-spin-Hall gap in single-layer 1T′ WSe_2 *Nat. Commun.* **9** 2003
[107] Qian X, Liu J, Fu L and Li J 2014 Quantum spin Hall effect in two-dimensional transition metal dichalcogenides *Science* **346** 1344–7
[108] Yan C, Zhang H, Weinert M and Li L 2020 Topological edge states at single layer WSe2 1T′-1H lateral heterojunctions *Appl. Phys. Lett.* **116** 203104
[109] Ugeda M M *et al* 2018 Observation of topologically protected states at crystalline phase boundaries in single-layer WSe_2 *Nat. Commun.* **9** 3401
[110] Quang T L *et al* 2018 Band-bending induced by charged defects and edges of atomically thin transition metal dichalcogenide films *2D Mater.* **5** 035034
[111] Liu L *et al* 2018 Termination-dependent edge states of MBE-grown WSe_2 *Phys. Rev.* B **98** 035034
[112] Zhao Y *et al* 2017 High-electron-mobility and air-stable 2D layered $PtSe_2$ FETs *Adv. Mater.* **29** 035034
[113] Yan M *et al* 2017 High quality atomically thin $PtSe_2$ films grown by molecular beam epitaxy *2D Mater.* **4** 045015
[114] Zhuang H L and Hennig R G 2013 Computational search for single-layer transition-metal dichalcogenide photocatalysts *J. Phys. Chem.* C **117** 20440–5
[115] Wang Y, Li L, Yao W, Song S, Sun J T, Pan J, Ren X, Li C, Okunishi E and Wang Y Q 2015 Monolayer $PtSe_2$, a new semiconducting transition-metal-dichalcogenide, epitaxially grown by direct selenization of Pt *Nano Lett.* **15** 4013–8
[116] Huang Z, Zhang W and Zhang W 2016 Band gap engineering of $PtSe_2$ arXiv:1605.08536
[117] Xu K, Chen P, Li X, Wu C, Guo Y, Zhao J, Wu X and Xie Y 2013 Ultrathin nanosheets of vanadium diselenide: a metallic two-dimensional material with ferromagnetic charge-density-wave behavior *Angew. Chem. Int. Ed.* **52** 10477–81
[118] Chen G *et al* 2020 Correlating structural, electronic, and magnetic properties of epitaxial VSe2 thin films *Phys. Rev.* B **102** 115149
[119] Ly T T, Duvjir G, Lam N H, Kim J, Choi B K and Chang Y J 2020 $\sqrt{3} \times 2$ and $\sqrt{3} \times \sqrt{7}$ charge density wave driven by lattice distortion in monolayer VSe_2 *J. Korean Phys. Soc.* **76** 412–25
[120] Duvjir G, Choi B, Ly T T, Lam N H, Chun S H, Jang K, Soon A, Chang Y J and Kim J 2019 Novel polymorphic phase of two-dimensional VSe_2: the 1T′ structure and its lattice dynamics *Nanoscale* **11** 20096
[121] Duvjir G, Kim J, Tsermaa B, Choi B K and Chang Y J 2020 151. Lattice dynamics driven by tunneling current in 1T′ structure of bilayer VSe_2 *J. Korean Phys. Soc.* **77** 1031–4
[122] Duvjir G, Choi B K, Ly T T, Lam N H, Jang K, Dung D D, Chang Y J and Kim J 2021 Multiple charge density wave phases of monolayer VSe_2 manifested by graphene substrates *Nanotechnology* **32** 115149
[123] Cheng P K, Tang C Y, Ahmed S, Qiao J, Zeng L H and Tsang Y H 2021 Utilization of group 10 2D TMDs-$PdSe_2$ as a nonlinear optical material for obtaining switchable laser pulse generation modes *Nanotechnology* **32** 055201
[124] Sun J, Shi H, Siegrist T and Singh D J 2015 Electronic, transport, and optical properties of bulk and mono-layer $PdSe_2$ *Appl. Phys. Lett.* **107** 153902
[125] Chow W L *et al* 2017 High mobility 2D palladium diselenide field-effect transistors with tunable ambipolar characteristics *Adv. Mater.* **29** 1602969
[126] Bartolomeo A D, Pelella A, Urban F, Grillo A, Iemmo L, Passacantando M, Liu X and Giubileo F 2020 Field emission in ultrathin PdSe2 back-gated transistors *Adv. Electron. Mater.* **6** 2000094
[127] Lei W, Zhang S, Heymann G, Tang X, Wen J, Zheng X, Hu G and Ming X 2019 A new 2D high-pressure phase of $PdSe_2$ with high-mobility transport anisotropy for photovoltaic applications *J. Mater. Chem.* C **7** 2096–105
[128] Kuklin A and Ågren H 2019 Quasiparticle electronic structure and optical spectra of single-layer and bilayer $PdSe_2$: proximity and defect-induced band gap renormalization *Phys. Rev.* B **99** 245114
[129] Oyedele A D *et al* 2017 $PdSe_2$: pentagonal two-dimensional layers with high air stability for electronics *J. Am. Chem. Soc.* **139** 14090–7
[130] Li E *et al* 2018 Construction of bilayer $PdSe_2$ on epitaxial graphene *Nano Res.* **11** 5858–65

[131] Zhang Y *et al* 2016 Electronic structure, surface doping, and optical response in epitaxial WSe_2 thin films *Nano Lett.* **16** 2485–91

[132] Fan P *et al* 2020 Epitaxial synthesis and electronic properties of monolayer Pd_2Se_3 *Chin. Phys.* B **29** 098102

[133] Duerloo K A N, Li Y and Reed E J 2014 Structural phase transitions in two-dimensional Mo- and W-dichalcogenide monolayers *Nat. Commun.* **5** 4214

[134] Park J C, Yun S J, Kim H, Park J H, Chae S H, An S J, Kim J G, Kim S M, Kim K K and Lee Y L 2015 Phase-engineered synthesis of centimeter-scale 1T′- and 2H-molybdenum ditelluride thin films *ACS Nano* **9** 6548–54

[135] Zhou L *et al* 2015 Large-area synthesis of high-quality uniform few-layer $MoTe_2$ *J. Am. Chem. Soc.* **137** 11892–5

[136] Li Y *et al* 2017 Room-temperature continuous-wave lasing from monolayer molybdenum ditelluride integrated with a silicon nanobeam cavity *Nat. Nanotechnol.* **12** 987–92

[137] Lin Y F *et al* 2014 Ambipolar $MoTe_2$ transistors and their applications in logic circuits *Adv. Mater.* **26** 3263–9

[138] Luo W, Zhu M, Peng G, Zheng X, Miao F, Bai S, Zhang X A and Qin S 2018 Carrier modulation of ambipolar few-layer $MoTe_2$ transistors by MgO surface charge transfer doping *Adv. Funct. Mater.* **28** 1704539

[139] Bie Y Q *et al* 2017 A $MoTe_2$-based light-emitting diode and photodetector for silicon photonic integrated circuits *Nat. Nanotech.* **12** 1124–9

[140] Li X, Dai Y, Niu C, Ma Y, Wei W and Huang B 2017 $MoTe_2$ is a good match for GeI by preserving quantum spin Hall phase *Nano Res.* **10** 2823–32

[141] Zhou L *et al* 2016 Synthesis of high-quality large-area homogenous 1T′ $MoTe_2$ from chemical vapor deposition *Adv. Mater.* **28** 9526–31

[142] Chen J, Wang G, Tang Y, Tian H, Xu J, Dai X, Xu H, Jia J, Ho W and Xie M 2017 Quantum effects and phase tuning in epitaxial hexagonal and monoclinic $MoTe_2$ monolayers *ACS Nano* **11** 3282–8

[143] Yu Y, Wang G, Qin S, Wu N, Wang Z, He K and Zhang X A 2017 Molecular beam epitaxy growth of atomically ultrathin $MoTe_2$ lateral heterophase homojunctions on graphene substrates *Carbon* **115** 526–31

[144] Song S, Keum D H, Cho S, Perello D, Kim Y and Lee Y H 2016 Room temperature semiconductor-metal transition of $MoTe_2$ thin films engineered by strain *Nano Lett.* **16** 188–93

[145] Rhodes D *et al* 2017 Engineering the structural and electronic phases of $MoTe_2$ through W substitution *Nano Lett.* **17** 1616–22

[146] Pham T T, Castelino R, Felten A and Sporken R 2020 Preparation of single phase 2H-$MoTe_2$ films by molecular beam epitaxy *Appl. Surf. Sci.* **523** 146428

[147] Kim J H, Kim K and Lee Z 2015 The hide-and-seek of grain boundaries from Moiré pattern fringe of two-dimensional graphene *Sci. Rep.* **5** 12508

[148] Pham T T, Castelino R, Felten A and Sporken R 2022 Study of surface oxidation and recovery of clean $MoTe_2$ films *Surf. Interfaces* **28** 101681

[149] Zhou X, Jiang Z, Zhang K, Yao W, Yan M, Zhang H, Duan W and Zhou S 2019 Electronic structure of molecular beam epitaxy grown 1 T′-$MoTe_2$ film and strain effect *Chin. Phys.* B **28** 107307

[150] Pham T T, Vancsó P, Szendrő M, Palotás K, Castelino R, Bouatou M, Chacon C, Henrard L, Lagoute J and Sporken R 2022 Higher-indexed Moiré patterns and surface states of $MoTe_2$/graphene heterostructure grown by molecular beam epitaxy *Npj 2D Mater. Appl.* **6** 48

[151] Zhao C *et al* 2020 Strain tunable semimetal-topological-insulator transition in monolayer 1T′-WTe_2 *Phys. Rev. Lett.* **125** 046801

[152] Tang S *et al* 2017 Quantum spin Hall state in monolayer 1T′-WTe_2 *Nat. Phys.* **13** 683–7

[153] Fei Z, Palomaki T, Wu S, Zhao W, Cai X, Sun B, Nguyen P, Finney J, Xu X and Cobden D H 2017 Edge conduction in monolayer WTe_2 *Nat. Phys.* **13** 677–82

[154] Jia Z Y *et al* 2017 Direct visualization of a two-dimensional topological insulator in the single-layer 1T′-WTe_2 *Phys. Rev.* B **96** 041108

[155] Lodge M S, Yang S A, Mukherjee S and Weber B 2021 Atomically thin quantum spin hall insulators *Adv. Mater.* **33** 2008029

[156] Song Y H *et al* 2018 Observation of coulomb gap in the quantum spin hall candidate single-layer 1 T′-WTe_2 *Nat. Commun.* **9** 4071

[157] Yan M *et al* 2017 Lorentz-violating type-II Dirac fermions in transition metal dichalcogenide $PtTe_2$ *Nat. Commun.* **8** 257

[158] Noh H J, Jeong J and Cho E J 2017 Experimental realization of type-II dirac fermions in a $PdTe_2$ superconductor *Phys. Rev. Lett.* **119** 01640

[159] Li E *et al* 2018 High quality $PdTe_2$ thin films grown by molecular beam epitaxy *Chin. Phys.* B **27** 2008029

[160] Peng J P, Guan J Q, Zhang H M, Song C L, Wang L, He K, Xue Q K and Ma X C 2015 Molecular beam epitaxy growth and scanning tunneling microscopy study of TiSe2 ultrathin films *Phys. Rev.* B **91** 121113

[161] Qian K *et al* 2020 Epitaxial growth and air-stability of monolayer Cu_2Te *Chin. Phys.* B **29** 018104

[162] Zhang X *et al* 2021 Room-temperature intrinsic ferromagnetism in epitaxial $CrTe_2$ ultrathin films *Nat. Commun.* **12** 809

[163] Lin H, Huang W, Zhao K, Lian C, Duan W, Chen X and Ji S H 2018 Growth of atomically thick transition metal sulfide films on graphene/6H-SiC(0001) by molecular beam epitaxy *Nano Res.* **11** 4722